Physics – Uspekhi **48** (4) 323 – 343 (2005)

REVIEWS OF TOPICAL PROBLEMS PACS numbers: **12.38.–t**, 12.38.Mh, **13.85.–t**, 25.75.Nq

Dense gluon matter in nuclear collisions

A V Leonidov

DOI: 10.1070/PU2005v048n04ABEH001890

Contents

Abstract. Theoretical and phenomenological aspects of the physics of high-energy heavy-ion collisions are reviewed with emphasis on ideas related to the theory and phenomenology of color glass condensate.

1. Introduction

A description of the physics of strong interactions and, in particular, of multiparticle production processes at high energies in the framework of quantum chromodynamics (QCD) requires a clean separation of perturbative and nonperturbative elements of the theory and their contribution to the description of the phenomenon under consideration. It is well known that a perturbative description in terms of the elementary excitations of the theory — quarks and gluons — is applicable only for the processes characterized by large energy – momentum transfer and, correspondingly, by small space – time scales. At large times (distances), the theory, if viewed in terms of quarks and gluons, is in the strong coupling regime. When moving from the weak towards the strong coupling regime, the original perturbative description should be enriched by new elements. In most cases, such an element is a soft background field, which encodes the part of nonperturbative information that has to be taken into account. In the new description, the elementary excitations are considered as propagating in this background field. Another possibility is directly introducing gluonic strings stretching between constituent quarks or gluons. Most often, a connection between perturbative and nonperturbative descriptions is built using the assumption of parton – hadron duality, which allows comparing calculations of the same physical quantities made in quark – gluon and hadronic terms. A classic example of this kind is the calculation of the characteristics of hadronic resonances (e.g., the ρ-meson) using the QCD sum rules.

The main topic of the present review is the theory and phenomenology of multiparticle production processes in nuclear collisions analyzed in the framework of a semiclassical approach developed in the last decade — the physics of color glass condensate (CGC) (see, e.g., recent reviews [1 – 3]). The CGC approach is based on a resummation technique in the QCD perturbation theory. In other approaches to describing the high-energy nuclear collisions, one either simultaneously takes both soft (nonperturbative) and hard (perturbative) degrees of freedom into account by combining them within basic Glauber collision geometry [4] or puts the main emphasis on the physics of gluon strings stretched in between the fast constituent degrees of freedom [5, 6]. Much attention is also paid to the statistical approach for describing high-energy collisions. In this case, a key role is played by the mechanism of transformation of the partonic matter into the hadronic one through a confinement – deconfinement phase transition. A detailed analysis of the physics of this transition can be found in Ref. [7]. Multiparticle production in high-energy nuclear collisions is drawing increased attention, in particular, due to new interesting experimental results obtained at the Relativistic Heavy Ion Collider (see, e.g., the forthcoming book [8]).

We also stress that many aspects of the physics of multiparticle production at high energies are universal, and therefore comparison with the results for $e^+ - e^-$ annihila-

A V Leonidov Lebedev Physics Institute, Russian Academy of Sciences, Leninskiĭ prosp. 53, 119991 Moscow, Russian Federation,
Russian Federation State Scientific Center 'Institute for Theoretical and Experimental Physics',
ul. B. Cheremushkinskaya 25, 117259 Moscow, Russian Federation
Tel. (7-095) 132 29 29. E-mail: leonidov@td.lpi.ru

Received 20 April 2004, revised 19 July 2004
Uspekhi Fizicheskikh Nauk **175** (4) 345 – 366 (2005)
Translated by A V Leonidov; edited by A M Semikhatov

tion [9 – 11] or hadron collisions [12] is always interesting and relevant [13]. What is specific to nuclear collisions is the very large density of primordial gluonic modes due to A-dependent (where A is the nucleus atomic number) amplification of the universal perturbative growth of the gluon density at high energies.

The present review attempts to give a balanced view of both theoretical and phenomenological aspects of ultrarelativistic heavy-ion physics in the context of a semiclassical picture related to CGC.

1.1 Theoretical developments

Quantum chromodynamics, a non-Abelian gauge theory, is a universally recognized theory of strong interactions. What is unusual about QCD is that it is formulated in terms of colored degrees of freedom, quarks and gluons, which are not observed in free state due to confinement of color. A rigorous description of the corresponding physical picture has not been worked out yet, and in applying QCD to the analysis of scattering processes at high energies, one therefore has to combine calculations based on the QCD Lagrangian with phenomenological considerations. In pre-QCD times, a basis for describing hadronic processes at high energies was the parton model. A modern physical picture in which the scattering process is formulated in terms of quark and gluon fields, on which QCD action depends, is termed the QCD – parton model. As follows from the term itself, the partonic degrees of freedom in the QCD – parton model are quarks and gluons. In spite of some principal restrictions related to the technical realization of the QCD – parton model (the special role of axial and planar gauges, different descriptions of scattering process in different frames of reference), it currently constitutes a no-alternative standard language for describing scattering processes at high energies.

The main goal of the present review is to describe, within a gauge theory of strong interactions, QCD, various characteristics of scattering processes with high-energy hadrons and nuclei characterized by the high density of partonic modes participating in the interaction at its early stage.

As an example, we consider a scattering of a color probe, a quark – antiquark dipole, on a hadronic (nuclear) target. Within the QCD – parton model, this process is described in terms of scattering of the quark and antiquark in the color dipole on quarks and gluons in the target, possibly accompanied by the creation of new gluons and quarks. The cross section of the scattering of a probe on the target depends on the kinematical characteristics of the process (e.g., on longitudinal and transverse momenta of the probe). In terms of the target parton modes, this means that probes having different sizes 'see' different partonic configurations in the target. The changes in partonic configurations (parton density) with the changing characteristic scale of the process (kinematical characteristics of the probe) is described by QCD evolution equations. In particular, the evolution of partonic densities with the changing transverse momentum of the probe is described, in the leading logarithmic approximation (LLA) in perturbation theory, by the Dokshitzer – Gribov – Lipatov – Altarelli – Parisi (DGLAP) equations [14], and that with the changing longitudinal momentum by the Balitsky – Fadin – Kuraev – Lipatov (BFKL) equation [15].

To construct a consistent theoretical formalism applicable at high energies, it is necessary to provide a description for nonlinear effects for correlators of color excitations in the dense partonic medium. Physically, the above necessity is related to the fact that as the collision energy grows, the partons in the target fill the impact parameter plane more and more densely and, starting with some energies, the linear approximation in density is no longer applicable [16].

Technically, the necessity of constructing a nonlinear generalization of the linear evolution equations is particularly clear in the case of the LLA in energy, where a solution of the BFKL equation, which sums leading logarithmic contributions, corresponds to a cross section characterized by a power-like growth at asymptotically high energies — a result contradicting the requirement of the unitarity of the theory and, at the very least, showing the insufficiency of the linear approximation for understanding the high-energy asymptotics of QCD. A natural line of research in this situation is to account for corrections nonlinear in parton density that are responsible, for example, for mutual screening of target partons at high partonic densities. The qualitative importance of such nonlinear effects and first quantitative calculations were made in the pioneering work [16]. In particular, quadratic nonlinearity in parton density, in the doubly logarithmic approximation (a regime of high energies and large transferred momenta), in which terms of the form $O(\alpha_s \log p_\perp^2 \log s)$ are kept (where α_s is the coupling constant of strong interactions, $p_\perp$ is the transverse momentum, and s is the collision energy squared) was first considered in Ref. [16], and the coefficient at the nonlinear term was calculated in Ref. [17]. The phenomenological aspects of physics related to the nonlinear contributions were discussed, e.g., in reviews [18, 19].

A logically complete description of high-energy QCD asymptotics in terms of auxiliary reggeon degrees of freedom in the cross t-channel was proposed by L N Lipatov (see review [20] and the references therein). We note that a description of QCD in reggeon terms arises via a very special resummation of self-energy (virtual) contributions to the propagator of gluons exchanged between the scattering particles. In particular, in Ref. [21], an effective action including both gluonic and reggeon degrees of freedom was constructed. We note that an interrelation between the results obtained in the reggeon approach and in the approach of the Wilson renormalization group (RG) discussed in the present review (in which reggeon degrees of freedom are not considered) remains unclear at present. This question seems to present a very important topic for further studies. An important step in this direction was made in a recent paper [22], in which the Balitsky – Kovchegov equation (see below, Section 3.3.3) was derived within the reggeon formalism. This equation has thus by now been derived in all the approaches used (operator expansion, Wilson RG, dipole model, and reggeon).

The rapid growth of the number of gluonic degrees of freedom that must be used in describing the physics of semihard processes with strong interactions leads to the idea of using a semiclassical (tree-level) description of the configuration of color fields in nuclei as a basic building block in the theory of high-energy processes [23]. The necessity of the collective treatment of gluon modes in the large-density regime naturally leads to a picture of disordered color glass condensate[1] as a characteristic state of gluon matter in this

[1] We note that in this case, the term 'condensate' is used to describe a system of gluon modes having parametrically large occupation numbers and is not related to the appearance of a new order parameter.

limit. A description in terms of the CGC arises for fast hadrons (nuclei) propagating with a speed close to the speed of light. Because of the Lorentz contraction, they are observed as thin disks propagating along the light cone. The corresponding formalism is realized as a two-dimensional classical effective theory valid in some interval of the Bjorken variable $x = p^+/P^+$, where P^+ is the longitudinal momentum of the nucleus and p^+ is that of the parton. The physical content of the model is specified by describing the source of the classical gluon field. The McLerran – Venugopalan (MV) model [23] suggests considering the partons (constituent quarks and hard gluons) as such sources, carrying a substantial part of the longitudinal momentum of the nucleus. These sources generate a soft gluon field, i.e., gluon modes with small x in the nuclear wave function. The validity of the classical description is related to the large occupation numbers $\sim 1/\alpha_s$, where $\alpha_s \equiv g^2/4\pi$ is the strong coupling constant and g is a color charge, and hence the corresponding gluon configurations can be described in terms of strong classical gluon fields[2] $\mathcal{A}^i \sim 1/g$ [cf. Section 2.2, Eqn (9)]. The physical picture behind the CGC is akin to the one considered in the physics of disordered magnetic systems. More precisely, averaging over the configuration of fast color sources, i.e., constituent quarks and hard gluons generating the soft gluon field, has to be performed *after* computing the correlators of quantum gluon modes. It is thus completely analogous to averaging over disorder in disordered magnets.

The McLerran – Venugopalan model provides, by construction, a tree-level classical description of the gluon field generated by constituent sources in the nucleus. In the low-density (large transverse momentum) limit, its results reproduce the corresponding lowest-order calculations in perturbative QCD. In the limit of high density of the source (small transverse momentum), the model predicts a *saturation* of the gluon distribution. A change in the behavior of the gluon distribution preventing its uncontrollable 'perturbative' growth at small transverse momenta occurs at a new important scale of the theory, the saturation momentum Q_s. The corresponding physical picture was (in terms of triple-pomeron interaction) first considered in Ref. [16]. A semi-classical interpretation of the saturation phenomenon was suggested in Ref. [24] and later confirmed in Ref. [25].

The considered effective theory is valid for some restricted interval of x. To analyze the contribution of gluon modes with smaller x, it is necessary to shift the scale of the effective theory (the characteristic longitudinal momentum of the sources) closer to the physical scale of the process $p^+ \ll P^+$ determined by the corresponding kinematical characteristics of the probe. This shift is realized via integration over the quantum fluctuations of the gluon modes in the kinematic interval that 'opens' due to the shift of the scale. Technically, the arising procedure is described in terms of the Wilson RG with an evolution in rapidity, first considered in Ref. [24]. Carrying out calculations to all orders in density requires computing the exact propagator (in terms of the external field) of quantum fluctuations in the corresponding background field. The problem is technically quite complex and was addressed in a number of publications [24, 26 – 31].

Historically, the major step that had to be made to finalize the development of the formalism introduced in Refs [23, 24, 26] was the construction of the correct effective action, from which it should have been possible to reproduce the BFKL evolution equation in the linear limit. Such an action was constructed in Ref. [32], where it was shown that in addition to the usual Yang – Mills term S_{YM}, the effective action in question contains an additional contribution S_W describing a nonlinear eikonal interaction of the current of fast sources J^+ with *quantum* fluctuations of the gauge potential A^- (at tree level, $A^- = 0$). It is important to note that the contribution of one-loop diagrams, which, for simplicity, we call virtual in what follows, to the BFKL equation arises precisely due to these nonlinear interactions.[3] We also mention Ref. [34], where an action analogous to that proposed in Ref. [32] was derived by considering a physically transparent picture of a system of precessing color spins and gluon fields.

The next step in understanding the nonlinear effects in QCD at high energies was made in Ref. [35], where a general functional evolution equation was derived in the LLA. This equation allows writing a coupled chain of evolution equations for parton correlators of an arbitrary order. It was proven that for a full description of nonlinear effects in the LLA, one must calculate two kernels of the nonlinear evolution equation, the virtual (corresponding to the contribution of diagrams with a virtual loop) $\sigma(x_\perp)$ and real (corresponding to the contribution of diagrams describing radiation of a real gluon) $\chi(x_\perp, y_\perp)$, which are nonlinear functionals of the background gluon field and generalize the corresponding kernels of the linear BFKL evolution equation. The general evolution equation first obtained in Ref. [35] was subsequently derived in a number of ways [29, 30, 36, 37]. We note that in the limit of linear kernels, the obtained chain of evolution equations formally coincides with that given by the well-known Bartels – Kwiecinski – Praszalowicz (BKP) equation, obtained within the reggeon formalism [38].

The first explicit calculation of the kernels $\sigma(x_\perp)$ and $\chi(x_\perp, y_\perp)$ was published in Ref. [27]. In this review, we describe the calculations in Refs [28 – 30]. We note that the answers obtained in [27] and [28 – 30] differ, at least in the light-cone gauge and infinite momentum frame. The source of this discrepancy is still unclear. It was shown [30, 39], however, that after a transformation to the covariant gauge and a coordinate transformation to the rest frame of the target, the equations in Refs [40, 41] are reproduced. This makes the difference between the results for the kernels obtained in [27] and [28 – 30] quite intriguing.

In the process of working out the answer for the evolution equation kernels, a number of results elucidating the general structure of the application of the Wilson RG formalism to the QCD parton model were derived in Refs [28 – 30]. In particular, a formulation of the QCD parton model on a complex time contour, required by the presence of time-dependent eikonal interactions, was constructed in Ref. [28]. This formulation allowed the elucidation of a symmetry structure of the problem and gave a rigorous definition of parton correlators as equal-time Wightman functions analogous to those considered in many-body physics. It was

[2] The term 'strong field' is used here in the context of the diagram technique, where the Green's functions of the fields $\mathcal{A}^i$ 'cancel' some of the factors of g in the diagrams' vertices, thereby changing the structure of the perturbation theory.

[3] One can show that within the same technique, the 'usual' DGLAP equation, corresponding to evolution in transverse momenta, can also be reproduced [33]. For this derivation, only the linear contribution from the eikonal term is needed. But the structure of the RG is in this case more complicated and requires further analysis.

proven, in particular, that in the LLA approximation, a real-time formulation of the theory can be used.

The results of the explicit analytical calculations in Refs [27, 29, 30] allowed comparing the evolution of quantum correlators in the Wilson RG with evolution equations obtained earlier in the framework of the operator product formalism [40] and by explicitly calculating Feynman diagrams in the dipole model formalism [41] and to prove their equivalence. We note that the nonlinear effects considered in Refs [40, 41] are in essence related to the colorless reggeon vertex $2 \to 4$ (triple-pomeron interaction).

An extensive analysis of the solutions of the nonlinear renormalization group evolution equation has revealed a number of important and interesting features [42 – 48]. The first and, probably, most important conclusion is that quantum corrections do not change the basic pattern of nonlinear saturation effects predicted at the tree level by the McLerran – Venugopalan model. The effects related to quantum evolution reveal themselves through the dependence of the saturation momentum Q_s on energy and transverse momentum. A second important result described in Refs [44, 45] is the construction of an effective description for all densities (transverse momenta) in the Gaussian (mean-field) approximation, in which one only has to specify a two-point function related to averaging over the sources, providing a smooth interpolation between the low-density and high-density limits.

As mentioned above, a key question addressed by the resummation program of QCD at high energies is how to work out a solution to the problem of a perturbative unitarity violation. Of course, it is not clear a priori whether a purely perturbative solution exists or whether taking effects of all orders in density in the leading logarithmic approximation into account through the above-described nonlinear evolution equation suffices. A detailed analysis of this problem was recently performed in Ref. [49] (in the double-logarithmic approximation) and in Refs [50 – 53]. It turned out that the derived nonlinear evolution equation solves the problem of unitarity violation only for fixed impact parameter scattering. It looks quite plausible that the solution to the problem is, after all, intrinsically nonperturbative. The reason for this conjecture is the necessity of generating a mass gap in the spectrum providing an exponential decay of the amplitude in the impact parameter plane and, correspondingly, a fulfillment of the Froissart bound [see Section 3.4, Eqn (83)]. In non-Abelian theories such as QCD, this is an absolutely nonperturbative phenomenon.

1.2 Applications to phenomenology

The key question of the physics of the dense parton medium is the quantitative understanding of the role of perturbative degrees of freedom in the early dynamics of nuclear reactions. A clear example of a formalism where the hard dynamics can be separated from the soft one is the physics of QCD jets, where the hard primordial parton subprocesses lead to the appearance of well-collimated fluxes of hadrons in the final state. But the practical aspects of the experimental detection of these fluxes imposes significant restrictions on studying the kinematics of primordial parton scattering (the corresponding minimal transverse momentum is equal to 50 – 100 GeV, see, e.g., [4, 19]). The temptation to generalize the perturbative approach to smaller transverse momenta leads to the formulation of the minijet approach to multiparticle production at high energies, described in detailed reviews [4, 19]). The main (quite radical) assumption of minijet physics is the existence of a direct link between the lowest-order perturbative diagrams and the inelastic cross section, which allows estimating the *number* of partons that took part in forming the transverse energy flow. Because of the infrared divergence of the basic $2 \to 2$ cross section, the dominant part of the thus calculated perturbative contribution to the inelastic cross section comes from the vicinity of the infrared cutoff, which has to be introduced 'by hand'. The calculations carried out in the framework of the minijet philosophy [54 – 57] played a decisive role in early estimates of the possibility of producing a dense and hot partonic matter at the early stages of nuclear collisions. The estimates of the number of minijet gluons made in Refs [54 – 57] were technically based on using the lowest-order parton rescattering mechanism and collinear factorization. The necessity of considering multiple binary collisions in the same event led to the necessity of using nonrigorous schemes like eikonal unitarization [58].

The special role of minijets in articulating the physical picture of early parton dynamics explains the interest in a more detailed analysis of their possible participation in forming the inelastic cross section. Rigorous perturbative calculations can be carried out only for infrared-stable observables (see, e.g., Ref. [59]), for which, if one neglects nonperturbative contributions, the predicted behavior of the physical observable is fully determined by the perturbation theory. Because minijet partonic degrees of freedom cannot be observed as well-collimated fluxes of hadronic transverse energy, it is natural to consider [60] the infrared stable quantity of transverse energy flow into a fixed rapidity window. This calculation can be done to the next-to-leading order accuracy [60]. A detailed analysis of the anatomy of the transverse energy flow in hadronic collisions [61] made using the HIJING generator [62] shows the dominant role of nonperturbative degrees of freedom at transverse energies of the order of several dozen GeV. An interesting quantity that allows separating the semihard and soft contributions to the inelastic cross section is the azimuthal asymmetry of the transverse energy flow analyzed in Refs [63, 64]. The main idea of these papers is that due to the basic character of semihard and soft mechanisms, an angular asymmetry in the transverse energy flow can arise only from the contribution of the semihard mechanism, thus allowing one to single out the perturbative contribution.

In the traditional approach to the description of nuclear scattering, perturbative and nonperturbative components were considered simultaneously, thus combining the semihard minijet and soft stringy contributions. Most applications were developed in the framework of corresponding Monte Carlo generators HIJING [62] and PYTHIA [65]. One of the most spectacular results obtained within this approach was the discovery of the sharply inhomogeneous turbulent nature of the gluon transverse energy release described in Ref. [66].

As already mentioned in Section 1.1, the modern understanding of the physics of high-energy nuclear collisions is based on the important role of nonlinear interactions in a dense parton medium. The analysis of the role of such effects in transverse energy production via minijets was first made in Ref. [57]. The main ingredient of the physical picture of transverse energy release in high-energy nuclear collisions considered in Ref. [57] was the statement that the dominant contribution to the transverse energy initially produced in these collisions comes from minijets having transverse

momenta of the order of the saturation scale. This hypothesis constitutes the foundation of the modern phenomenology of primordial parton dynamics in heavy-ion collisions based on the physics of saturation.

The physical scenario outlined in Ref. [57] was analyzed, from various standpoints, in Refs [67–73]. One of the main areas of research was the development of a tree-level description of gluon production, generalizing the formalism of the MV model in calculations of gluon production. The first complete calculation of gluon production in the collision of two nuclei of the lowest order in gluon density was done in Ref. [67]. Along the lines of [25], the problem of finding the gluon spectrum in nuclear collisions to all orders in density was solved in Ref. [70]. Much attention was paid to the numerical analysis of the gluon production in nuclear scattering [74–81]. This approach is intrinsically non-perturbative and very promising.

The experimental data obtained at RHIC [82–85] made it possible to test the main prediction of CGC physics in the RHIC regime [86–90]. One of the most interesting questions arising in describing the physics of the early stages of nuclear collisions is the role of rescattering of initially produced gluons. In recent papers [89, 91–93], this question was analyzed in detail in the framework of the saturation CGC physics, including, in Ref. [89], a fairly detailed scenario going beyond the binary scattering approximation.

The general conclusion is that the experimental data are in qualitative agreement with the CGC-inspired models. We note, however, that a transverse scale characteristic for parton production at RHIC energies looks somewhat small to consider the use of perturbation theory reliable.

2. Tree-level description: the McLerran–Venugopalan model

2.1 Physical picture

We start by describing a physical picture of a heavy nucleus in the framework of the QCD–parton model mentioned in Section 1. We consider a nucleus moving along the z axis having the 4-momentum $P^\mu = (P^0, 0, 0, P^z)$. When describing ultrarelativistic particles, it is convenient to introduce the so-called light-cone coordinates. For the cartesian 4-vector v^μ, the light-cone coordinates are $v^\mu = (v^+, v^-, \mathbf{v}_\perp)$, where $v^+ \equiv (1/\sqrt{2})(v^0 + v^3)$, $v^- \equiv (1/\sqrt{2})(v^0 - v^3)$, and $\mathbf{v}_\perp \equiv (v^1, v^2)$. The scalar product is given by $p \cdot x = p^+x^- + p^-x^+ - p_\perp \cdot x_\perp$, where p^- and p^+ are the energy and the longitudinal momentum, and x^+ and x^- are the light-cone time and the longitudinal coordinate, respectively.

A description of the interacting matter in the nucleus related to the QCD picture divides partonic (quark and gluon) modes into two basic categories. The first includes hard partons (valence quarks and hard gluons), which carry a significant part of the light-cone momentum P^+ and are characterized, in the leading approximation, by free motion along the longitudinal z axis (such that their momenta are collinear to P^+). Hard partons serve as sources for gluons with parametrically small longitudinal momenta $q^+ \ll P^+$ (soft modes).

At the heart of the RG approach discussed in Section 3 lies a separation of the gluon modes in the nuclear wave function into 'soft' and 'hard' (fields and their sources) by comparing their longitudinal momentum p^+ with some characteristic longitudinal scale Λ^*, such that $p^+ > \Lambda^*$ for the hard modes and $p^+ < \Lambda^*$ for the soft ones. The scale $\Lambda^* = x_* P^+$ should be such that x_* should not be too small. In fact, the Wilson RG procedure described in Section 3 ascribes the gluon modes with $x \lesssim x_*$ to sources, and those with $x > x_*$ to the fields. The goal of the RG approach is a quantitative analysis of the physics of gluon modes with $x_* > x$. We recall that the Bjorken x variable characterizes the longitudinal scale of a probe interacting with the nucleus. A key particularity of the small-x domain $x \ll 1$ is the dominance of gluons in the wave function of a projectile.

At small x (high energies), the occupation numbers characterizing the soft gluon modes are big. This explains the starting point of the main idea of the MV model, which is to describe these soft gluon modes by the tree-level classical Weizsäcker–Williams color radiation A_a^μ (the subscript a refers to a color of the gluon mode) of hard partons, which are in turn characterized by a static random color charge density ρ_a. The physical picture corresponding to such separation of scales can be described as follows.

The fast partons having large longitudinal momenta p^+ propagate along the light cone emitting and absorbing soft gluons. In the eikonal approximation, this corresponds to having one nonzero component of the radiating current in the $+$ direction, $J_a^\mu = \delta^{\mu+} J_a^+$. The hard partons are delocalized in the longitudinal coordinate x^- at distances $\Delta x^- \sim 1/p^+$ and appear (almost) point-like for soft radiation. Of principal importance is also a hierarchy of temporal scales. For modes close to the mass shell, $2p^+p^- \sim p_\perp^2$, and hence, according to the uncertainty relation, *soft* gluons have large energies (frequencies) $p^- \sim p_\perp^2/p^+$ and, correspondingly, short lifetimes

$$\Delta x^+ \sim \frac{1}{p^-} \sim \frac{p^+}{p_\perp^2} \sim \frac{xP^+}{p_\perp^2}\,.$$

At such small lifetimes, the dynamics of hard modes is effectively frozen, and therefore soft gluons are effectively coupled to the static correlators of the hard modes.

The current describing the hard modes can thus be written as

$$\begin{aligned} &J_a^\mu(x) = \delta^{\mu+}\rho_a(x^-, \mathbf{x}_\perp)\,, \qquad \partial^-\rho_a \equiv \frac{\partial \rho_a}{\partial x^+} = 0\,, \\ &\operatorname{supp}\rho_a = \left\{ |x^-| \leqslant \frac{1}{\Lambda^+} \right\}. \end{aligned} \tag{1}$$

In the non-Abelian equations of motion describing the tree-level dynamics of soft gluons, current (1) plays the role of a source,

$$[\mathrm{D}_\nu, F^{\nu\mu}] = \delta^{\mu+}\rho_a(x^-, \mathbf{x}_\perp)\,, \tag{2}$$

where D_ν is the covariant derivative and $F^{\nu\mu}$ is the Yang–Mills field strength. The source ρ_a is a stochastic variable with zero mean. The spatial correlations $\rho_a(\mathbf{x})$ ($\mathbf{x} \equiv (x^-, \mathbf{x}_\perp)$) at the scale Λ^+ are inherited from (generally speaking, static) correlators of hard gluons. The weight of a given charge configuration ρ_a is determined by some functional $W_\Lambda[\rho]$ that is gauge invariant by assumption. An analysis of the gluon field generated by the source ρ_a is most transparent in the light-cone gauge $A^+ = 0$.

The calculation of gluonic correlators in the MV model proceeds in two steps:

• solving classical Yang – Mills equations (2) in the light-cone gauge $A^+ = 0$. The solution $\mathcal{A}^i(\mathbf{x})[\rho]$ is some nonlinear functional of ρ. In Section 2.2, we show that it is always possible to construct a static solution of (2) having $A^- = 0$.

• computing correlators in this classical solution by averaging with respect to ρ with the weight $W_\Lambda[\rho]$,

$$\left\langle A_a^i(x^+,\mathbf{x})A_b^j(x^+,\mathbf{y})\ldots\right\rangle_\Lambda = \int \mathcal{D}\rho\, W_\Lambda[\rho]\, \mathcal{A}_a^i(\mathbf{x})\mathcal{A}_b^j(\mathbf{y})\ldots, \tag{3}$$

where $\mathbf{x} \equiv (x^-, \mathbf{x}_\perp)$ and the normalization of correlators is fixed by

$$\int \mathcal{D}\rho\, W_\Lambda[\rho] = 1\,. \tag{4}$$

It is important to note that correlators (3) depend on the scale Λ^+. As is discussed in Section 2.2, the effective theory specified by Eqns (2) and (3) in fact holds only for the modes having longitudinal momenta not too small compared to the reference scale Λ^+. At very small longitudinal momenta $b\Lambda^+$ with $b \ll 1$, the (large) quantum corrections of the order of $\alpha_s \ln(1/b)$ have to be included. To calculate correlators at the new scale $b\Lambda^+$, one has to construct a new effective theory via integration over the quantum degrees of freedom with longitudinal momenta in the strip $b\Lambda^+ < |p^+| < \Lambda^+$.

2.2 Classical solution

Understanding the structure of the classical solution of (2) is a key to the physics of the MV model. Before turning to the non-Abelian case, it is useful to consider its Abelian simplification, i.e., to solve the equation $\partial_\nu \mathcal{F}^{\nu\mu} = \delta^{\mu+}\rho(\mathbf{x})$, where $\mathcal{F}^{\mu\nu}$ is now an Abelian field strength, in the light-cone gauge $A^+ = 0$. For the sought static solution, the $\mu = -$ and $\mu = i$ components of the equations of motion imply that $\mathcal{A}^- = 0$ (and hence $\mathcal{F}^{-+} = \mathcal{F}^{i-} = 0$) and $\mathcal{F}^{ij} = 0$. The sought static solution is thus a two-dimensional pure-gauge one,

$$\mathcal{A}^i(p) = -\frac{p^i}{p^+}\,\frac{\rho(p^+,p_\perp)}{p_\perp^2}\,. \tag{5}$$

To specify the solution completely (in particular, to provide its description in coordinate space) we must choose some prescription for the axial pole at $p^+ = 0$. We choose the prescription $1/p^+ \equiv 1/(p^+ + \mathrm{i}\varepsilon)$. In coordinate space, this leads to the solution in the form

$$\mathcal{A}^i(x^-, x_\perp) = \int_{-\infty}^{x^-} \mathrm{d}y^-\, \partial^i \alpha(y^-, x_\perp)\,, \tag{6}$$

vanishing at $x^- \to -\infty$. The function $\alpha(\mathbf{x})$ satisfies $-\nabla_\perp^2\alpha(\mathbf{x}) = \rho(\mathbf{x})$. Different prescriptions for the axial pole correspond to the same electric field $\mathcal{F}^{i+}(\mathbf{x}) = \partial^i\alpha(\mathbf{x})$ and thus to the prescription-invariant physics.

Turning now to the analysis of the non-Abelian case, we note that for a static charge density ρ, Eqns (2) are, generally speaking, not consistent. Indeed, from $\left[\mathrm{D}_\mu, [\mathrm{D}_\nu, F^{\nu\mu}]\right] \equiv 0$, there follows a covariant conservation of the color current $[\mathrm{D}_\mu, J^\mu] = 0$, and therefore the considered current $J^\mu = \delta^{\mu+}J^+$ must satisfy

$$[\mathrm{D}^-, J^+] \equiv \partial^- J^+ - \mathrm{i}g[A^-, J^+] = 0\,,$$

which (at $\mathcal{A}^- \neq 0$) it does not. The current is static only up to the isotopic precession

$$J^+(x^+,\mathbf{x}) = \mathcal{W}(x^+,\mathbf{x})\,\rho(\mathbf{x})\,\mathcal{W}^\dagger(x^+,\mathbf{x})\,,$$

where ρ is some initial orientation of the color charge density at some $x^+ = x_0^+$ and $\mathcal{W}[A^-]$ is a time-ordered Wilson line

$$\mathcal{W}[A^-](x^+,\mathbf{x}) \equiv \mathrm{T}\exp\left\{\mathrm{i}g\int_{x_0^+}^{x^+}\mathrm{d}z^+\, A^-(z^+,\mathbf{x})\right\}. \tag{7}$$

Analogously to the above-described Abelian case, we can, however, consider a static solution of the form

$$A^+ = A^- = 0\,, \qquad A^i \equiv \mathcal{A}^i(x^-, x_\perp)\,. \tag{8}$$

Solution (8) is invariant under gauge transformations independent of x^- and x^+, i.e., under two-dimensional transformations in the transverse plane. Then, for the $\mu = +$ component, we have $[\mathrm{D}_i, F^{i+}] = \rho(\mathbf{x})$, while for the $\mu = i$ one, we obtain $[\mathrm{D}_j, F^{ji}] = 0$, with the two-dimensional pure-gauge solution ($\mathcal{F}^{ji} = 0$)

$$\mathcal{A}^i(x^-, x_\perp) = \frac{\mathrm{i}}{g}\,U(x^-, x_\perp)\,\partial^i U^\dagger(x^-, x_\perp)\,, \tag{9}$$

where $U(x^-, x_\perp)$ belongs to $\mathrm{SU}(N)$ and has an implicit dependence on ρ. The fields $\mathcal{A}^i$ in (9) can be gauge-rotated to zero by a gauge transformation $U^\dagger(\mathbf{x})$,

$$\mathcal{A}^\mu \to \tilde{\mathcal{A}}^\mu = U^\dagger\mathcal{A}^\mu U + \frac{\mathrm{i}}{g}\,U^\dagger\,\partial^\mu U\,, \tag{10}$$

leaving the only nonzero component

$$\tilde{\mathcal{A}}^+ = \frac{\mathrm{i}}{g}\,U^\dagger(\partial^+ U)\,.$$

We note that the transformed gauge potential satisfies the covariant gauge constraint $\partial_\mu\tilde{A}^\mu = 0$ and the transformed equations of motion take the simple form $-\nabla_\perp^2\tilde{A}^+(\mathbf{x}) = \tilde{\rho}(\mathbf{x})$, where

$$\tilde{\rho}(\mathbf{x}) \equiv U^\dagger(\mathbf{x})\,\rho(\mathbf{x})\,U(\mathbf{x}) \tag{11}$$

is the classical charge density in the rotated gauge. It is convenient to introduce, by analogy to the Abelian case, a new function $\alpha(\mathbf{x}) \equiv \tilde{\mathcal{A}}^+(\mathbf{x})$, such that $\alpha(\mathbf{x})$ satisfies $-\nabla_\perp^2\alpha(\mathbf{x}) = \tilde{\rho}(\mathbf{x})$. In computing the gluon correlators, it is convenient to use an explicit expression for U in terms of α,

$$U^\dagger(x^-, x_\perp) = \mathrm{P}\exp\left\{\mathrm{i}g\int_{x_0^-}^{x^-}\mathrm{d}z^-\,\alpha(z^-, x_\perp)\right\}, \tag{12}$$

where P denotes ordering of the matrices $\alpha(\mathbf{x})$ from left to right in ascending (descending) order in x^- at $x^- > x_0^-$ ($x^- < x_0^-$), respectively. Various choices of x_0^- correspond to solutions related by residual two-dimensional gauge transformations. We have thus fully constructed a static classical solution $\mathcal{A}^i[\tilde{\rho}]$ in the light-cone gauge as an implicit nonlinear functional of the source $\tilde{\rho}$. Explicit construction of the solution is, obviously, not possible — one would have to explicitly solve the nonlinear equation $U[\rho](-\nabla_\perp^2\alpha)U^\dagger[\rho] = \rho$ for α. For hard modes, the source ρ is localized in the vicinity of $x^- = 0$ [cf. (1)].

We now turn to the all-important issue of fixing the residual gauge invariance. To do it at the tree level [i.e., on classical solution (9)], we again use the retarded boundary conditions in x^-: $\mathcal{A}^i(x^-, x_\perp) \to 0$ for $x^- \to -\infty$, which is equivalent to choosing $x_0^- \to -\infty$ in (12). The choice of this boundary condition fixes, in fact, the axial pole prescription for the gluon propagator used in computing the quantum corrections. We also note that the chosen retarded prescription corresponds to the source having its support only at positive x^- in the interval $0 \lesssim x^- \lesssim 1/\Lambda^+$.

In the MV approach, Λ^+ is a large longitudinal scale, and the dominant contribution to the target wave function and, correspondingly, cross section comes from the modes with the characteristic longitudinal size

$$\Delta x^- \sim \frac{1}{p^+} \gg \frac{1}{\Lambda^+} .$$

These modes are thus sensitive only to a crude longitudinal structure of the localized source, allowing us to simplify the classical solution at parametrically large distances from the source by using the following approximation for the rotation matrices:

$$U^\dagger(x^-, x_\perp) \equiv \mathrm{P}\exp\left\{ \mathrm{i}g \int_{-\infty}^{x^-} \mathrm{d}z^- \, \alpha(z^-, x_\perp) \right\} \approx \theta(x^-)\, \Omega^\dagger(x_\perp) + \theta(-x^-) , \tag{13}$$

where θ is the Heaviside theta-function,

$$\Omega^\dagger(x_\perp) \equiv \mathrm{P}\exp\left\{ \mathrm{i}g \int_{-\infty}^{\infty} \mathrm{d}z^- \, \alpha(z^-, x_\perp) \right\} , \tag{14}$$

and therefore [cf. (9)]

$$\mathcal{A}^i(x^-, x_\perp) \approx \theta(x^-)\, \frac{\mathrm{i}}{g}\, \Omega(\partial^i \Omega^\dagger) \equiv \theta(x^-) \mathcal{A}^i_\infty(x_\perp) , \tag{15}$$

and the chromoelectric field strength is effectively a delta-function,[4]

$$\mathcal{F}^{i+}(\mathbf{x}) \equiv -\partial^+ \mathcal{A}^i \approx -\delta(x^-)\, \mathcal{A}^i_\infty(x_\perp) . \tag{16}$$

To construct observable quantities from gauge potentials $\mathcal{A}$, we recall that a gluon component of the structure function $xG(x, Q^2)$ is related to the momentum density of gluons $\mathrm{d}N/\mathrm{d}^3k$ by

$$xG(x, Q^2) = \int \mathrm{d}^2k_\perp \, \mathrm{d}k^+ \theta(Q^2 - k_\perp^2) x\delta\left(x - \frac{k^+}{P^+} \right) \frac{\mathrm{d}N}{\mathrm{d}^3k} , \tag{17}$$

where $\mathrm{d}N/\mathrm{d}^3k$ can, in turn, be expressed through the correlator of gluon fields

$$\frac{\mathrm{d}N}{\mathrm{d}^3k} = \sum_\lambda \sum_c a^\dagger_{\lambda c}(\mathbf{k})\, a_{\lambda c}(\mathbf{k}) = \frac{2k^+}{(2\pi)^3} \left\langle A^i_c(x^+, \mathbf{k}) A^i_c(x^+, -\mathbf{k}) \right\rangle , \tag{18}$$

where averaging is performed over the wave function of a hadron (nucleus).[5] Relations (17) and (18) allow us to interpret (17) as a density of gluons with the longitudinal momentum $k^+ = xP^+$ and transverse momentum $|k_\perp| \leqslant |Q|$ in the hadron (nuclear) wave function.

Therefore, a tree-level (i.e., calculated on the classical solution) structure function $xG_{\mathrm{cl}}(x, Q^2)$ has the form

$$xG_{\mathrm{cl}}(x, Q^2) = \frac{1}{\pi} \int \frac{\mathrm{d}^2k_\perp}{(2\pi)^2}\, \theta(Q^2 - k_\perp^2) \left\langle \left| \mathcal{F}_a^{i+}(\mathbf{k}) \right|^2 \right\rangle_\Lambda , \tag{19}$$

where averaging over ρ is done at the scale $\Lambda^+ \sim xP^+$ [see (3), (4)]. In the linear approximation in ρ (weak-field limit), we have $\mathcal{F}_a^{+j} \simeq \mathrm{i}(k^j/k_\perp^2)\rho_a$ and, therefore,

$$xG_{\mathrm{cl}}(x, Q^2) \simeq \frac{1}{\pi} \int \frac{\mathrm{d}^2k_\perp}{(2\pi)^2}\, \frac{\theta(Q^2 - k_\perp^2)}{k_\perp^2} \left\langle \left| \rho_a(\mathbf{k}) \right|^2 \right\rangle_\Lambda . \tag{20}$$

We note that in the considered approximation, the dependence of the gluon density on x is only due to the x-dependence of the weight functional $W_\Lambda[\rho]$ ($\Lambda^+ \sim xP^+$), and hence all x-dependence in the MV model is encoded in the weight functional and determines, in effect, its (quantum) evolutionary dependence on Λ^+.

We note that (19) allows a natural interpretation in terms of the gluon number density in the transverse momentum plane in the unit of rapidity $\tau = \ln P^+/\Lambda^+ \equiv \ln 1/x$:

$$xG_{\mathrm{cl}}(x, Q^2) \simeq \int^{Q^2} \mathrm{d}^2k_\perp \, \frac{1}{4\pi^3} \left\langle \left| \mathcal{F}_a^{i+}(\mathbf{k}) \right|^2 \right\rangle_\Lambda \equiv \int^{Q^2} \mathrm{d}^2k_\perp \, \frac{\mathrm{d}N}{\mathrm{d}\tau \, \mathrm{d}^2k_\perp} . \tag{21}$$

An important role is played in what follows by the gluon number density in the transverse phase space parameterized by the so-called unintegrated structure function $\varphi(x, k_\perp^2)$. For a homogeneous (in the sense of density dependence on the impact parameter) domain in the transverse plane with an area $S_\perp$, the functions $xG_{\mathrm{cl}}(x, Q^2)$ and $\varphi(x, Q^2)$ are related by

$$xG_{\mathrm{cl}}(x, Q^2) \equiv \frac{N_\mathrm{c}^2 - 1}{4\pi^3}\, S_\perp \int^{Q^2} \mathrm{d}^2k_\perp \, \frac{4\pi^3}{N_\mathrm{c}^2 - 1} \frac{1}{S_\perp} \frac{\mathrm{d}N}{\mathrm{d}\tau \, \mathrm{d}^2k_\perp} = \frac{N_\mathrm{c}^2 - 1}{4\pi^3}\, S_\perp \int^{Q^2} \mathrm{d}^2k_\perp \, \varphi(x, k_\perp^2) , \tag{22}$$

where N_c is the number of colors.

2.3 Gluon distribution in the McLerran – Venugopalan model of the nucleus: low-density limit

The simple model of the color source generating the gluonic component of the nuclear wave function proposed by McLerran and Venugopalan [23] corresponds to considering the $A \times N_\mathrm{c}$ constituent quarks in the nucleus as an ensemble of *independent* color sources. The main approximation made in this model clearly neglects correlations between the colors of constituent quarks belonging to the same nucleon due to confinement. For sufficiently small probes and sufficiently large nuclei, this should be a good approximation. The total color charge in the tube with the transverse cross section $\Delta S_\perp$ is described by its moments,

$$\langle Q^a \rangle = 0 , \quad \langle Q^a Q^a \rangle = \Delta S_\perp \frac{g^2 C_\mathrm{F} N_\mathrm{c} A}{\pi R_A^2} \equiv \Delta S_\perp \frac{g^2 (N_\mathrm{c}^2 - 1) A}{2\pi R_A^2} , \tag{23}$$

[4] We note that δ- and θ-functions in these formulas are understood as being regularized at distances $\Delta x^- \sim 1/\Lambda^+$.

[5] In Eqn (18), $a^\dagger_{\lambda c}(\mathbf{k})$ and $a_{\lambda c}(\mathbf{k})$ are creation and annihilation operators of a gluon with momentum $\mathbf{k}$, color c, and transverse polarization λ.

and for the color charge density Q^a, we therefore have

$$\frac{\langle Q^a Q^a\rangle}{\Delta S_\perp (N_c^2-1)} = \frac{g^2}{2}\,\frac{A}{\pi R_A^2} \equiv \mu_A^2 . \tag{24}$$

In terms of $\rho^a(x^-, x_\perp)$,

$$\begin{aligned} Q^a &= \int_{\Delta S_\perp} \mathrm{d}^2 x_\perp \int \mathrm{d}x^-\, \rho^a(x^-, x_\perp) \\ &\equiv \int_{\Delta S_\perp} \mathrm{d}^2 x_\perp\, \rho^a(x_\perp) , \end{aligned} \tag{25}$$

while the moments of color charge distribution (23) correspond, assuming homogeneity in the impact parameter plane, to the correlators

$$\begin{aligned} &\left\langle \rho^a(x^-, x_\perp)\, \rho^b(y^-, y_\perp)\right\rangle = \delta^{ab}\delta(x_\perp - y_\perp)\,\delta(x^- - y^-)\lambda_A(x^-) , \\ &\left\langle \rho^a(x_\perp)\, \rho^b(y_\perp)\right\rangle = \delta^{ab}\delta(x_\perp - y_\perp)\,\mu_A^2 \end{aligned} \tag{26}$$

or, in momentum space,

$$\left\langle \rho^a(k_\perp)\, \rho^a(-k_\perp)\right\rangle = \pi R_A^2\, \mu_A^2 , \tag{27}$$

where $\mu_A^2 \equiv \int \mathrm{d}x^- \lambda_A(x^-) = g^2 A/2\pi R_A^2$ [see (24)]. The weight functional generating correlators (26) is, evidently, Gaussian:

$$W_A[\rho] \sim \exp\left[-\frac{1}{2}\int \mathrm{d}^3 x\, \frac{\rho_a(\mathbf{x})\rho_a(\mathbf{x})}{\lambda_A(x^-)}\right] . \tag{28}$$

Using (20) and (26), we obtain an expression for the structure function $xG_{\mathrm{cl}}(x, Q^2)$,

$$\begin{aligned} xG_{\mathrm{cl}}(x, Q^2) &\simeq \frac{N_c^2 - 1}{4\pi}\, R_A^2\, \mu_A^2 \int_{\Lambda_{\mathrm{QCD}}^2}^{Q^2} \frac{\mathrm{d}k_\perp^2}{k_\perp^2} \\ &= A N_c\, \frac{\alpha_s C_F}{\pi} \ln \frac{Q^2}{\Lambda_{\mathrm{QCD}}^2} , \end{aligned} \tag{29}$$

where we immediately recognize the standard spectrum of gluons emitted by the AN_c quarks in the nucleus calculated in the lowest order in perturbation theory. From expressions (11), (27), and (29), it follows that in the considered weak-field approximation,

$$\varphi_A(x, k_\perp^2) = \frac{\mu_A^2}{k_\perp^2} . \tag{30}$$

2.4 Gluon distribution in the McLerran – Venugopalan model of the nucleus: saturation

In Section 2.3, we calculated the unintegrated structure function φ in the low-density regime. From the standpoint of calculational technique, 'low density' means neglecting the non-Abelian effects in computing the correlation of chromoelectric fields [see (19), (21)]. The fully non-Abelian calculation was performed in Refs [24, 25] (see also a detailed and transparent derivation in Ref. [2]). The answer for the unintegrated structure function $\varphi(x, k_\perp^2)$ takes the form

$$\begin{aligned} \varphi_A(k_\perp) = \frac{1}{\pi\alpha_s N_c} \int \frac{\mathrm{d}^2 x_\perp}{x_\perp^2} \exp\left(-\mathrm{i}k_\perp x_\perp\right) \\ \times \left[1 - \exp\left(-\frac{1}{4}x_\perp^2 Q_A^2 \ln\frac{1}{x_\perp^2 \Lambda_{\mathrm{QCD}}^2}\right)\right] , \end{aligned} \tag{31}$$

where

$$Q_A^2 \equiv \alpha_s N_c \mu_A^2 = \alpha_s N_c \int \mathrm{d}x^-\, \lambda_A(x^-) . \tag{32}$$

From (31), it is clear that the (transverse) momentum scale Q_s^2 at which nonlinear effects become important is determined by the nonlinear equation

$$Q_s^2 \simeq Q_A^2 \ln\frac{Q_s^2}{\Lambda_{\mathrm{QCD}}^2} , \tag{33}$$

where the characteristic transverse distance was chosen equal to $1/x_\perp^2 = Q_s^2$. The properties of nonlinear gluon distribution (31) are best illustrated by considering its asymptotics at small (large transverse momenta) and large (small transverse momenta) densities. It is easily seen that formula (31) interpolates between the following limits:

$$\varphi_A(k_\perp \gg Q_s) = \frac{\mu_A^2}{k_\perp^2} \to \varphi_A(k_\perp \ll Q_s) = \frac{1}{\alpha_s N_c} \ln\frac{Q_s^2}{k_\perp^2} . \tag{34}$$

Equation (34) demonstrates a key property of Eqn (31) at small momenta. The saturation phenomenon shows itself in a mild logarithmic infrared divergence as compared to the power-like infrared divergence in the perturbative regime. The scale of transverse momenta Q_s controlling this transition is called the saturation momentum. In turn, the structure function $xG(x, Q^2)$ calculated from (31) interpolates between the following limits:

$$\begin{aligned} &xG_A(x, Q^2)\,(k_\perp^2 \gg Q_s^2) \simeq N_c\, \frac{\alpha_s C_F}{\pi} \ln\frac{Q^2}{\Lambda_{\mathrm{QCD}}^2} , \\ &xG_A(x, Q^2)\,(k_\perp^2 \ll Q_s^2) \simeq \frac{1}{4\pi^3\alpha_s}\,\frac{N_c^2 - 1}{N_c}\,\pi R_A^2 \ln\frac{Q_s^2}{Q^2} . \end{aligned} \tag{35}$$

Regarding the second relation in (35), we note the inverse proportionality to the strong coupling constant α_s, which is typical of the physics of saturation.

3. Quantum corrections in the high-energy limit

In Section 2, we discussed the MV approach to the description of dense partonic systems at the tree-level (classical) approximation in QCD at high energies. In the present section, we describe a systematic approach to computing quantum corrections to the tree-level description.

3.1 Renormalization group

Quantum corrections to the tree-level MV picture are determined by the physics of quantum modes with longitudinal momenta $|p^+| < \Lambda^+$ considered in addition to the classical modes $\mathcal{A}^i$ generated by the source ρ. The restriction $|p^+| < \Lambda^+$ comes from the fact that, by assumption, the modes having $|p^+| > \Lambda^+$ were already integrated out in the process of constructing the effective theory at the scale Λ^+.

The basic object of the theory under construction is the generating functional of the correlators of gluon fields having longitudinal momenta in the interval $|p^+| < \Lambda^+$ in the light-cone gauge $A^+ = 0$:

$$\begin{aligned} \mathcal{Z}[j] = \int \mathcal{D}\rho\, W_\Lambda[\rho]\, Z_\Lambda^{-1}[\rho] \int^\Lambda \mathcal{D}A_a^\mu\, \delta(A_a^+) \\ \times \exp\left(\mathrm{i}S[A, \rho] - \mathrm{i}\int j\cdot A\right) \equiv \int \mathcal{D}\rho\, W_\Lambda[\rho]\, Z_\Lambda[\rho, j] . \end{aligned} \tag{36}$$

Equation (36) includes two functional integrations: over A^μ,

$$Z_\Lambda[\rho,j] \equiv Z_\Lambda^{-1}[\rho] \int^\Lambda \mathcal{D}A_a^\mu\, \delta(A_a^+) \exp\left(\mathrm{i}S[A,\rho] - \mathrm{i}\int j\cdot A\right), \tag{37}$$

where $Z_\Lambda[\rho] \equiv Z_\Lambda[\rho, j=0]$ describes quantum fluctuations at fixed ρ, and the classical averaging over ρ with the weight $W_\Lambda[\rho]$. The subscript Λ denotes integration over the modes having $|p^+| < \Lambda^+$.[6]

The quantum dynamics of the problem is specified by the effective action $S[A,\rho]$ such that, first, the tree-level equations of motion are reproduced in the regime $\delta S/\delta A^\mu = 0$ and, second, a correct quantum evolution of the correlators of the theory is ensured. Such an effective action was proposed in Refs [27, 32, 35] (see also Ref. [34]),

$$S[A,\rho] = -\int \mathrm{d}^4x\, \frac{1}{4} F^a_{\mu\nu}F_a^{\mu\nu} + \frac{\mathrm{i}}{gN_\mathrm{c}}\int \mathrm{d}^3\mathbf{x}\, \mathrm{Tr}\left\{\rho(\mathbf{x})\, \mathcal{W}_{\infty,-\infty}(\mathbf{x})\right\} \equiv S_\mathrm{YM} + S_\mathcal{W}, \tag{38}$$

where

$$\mathcal{W}_{\infty,-\infty}[A^-](\mathbf{x}) = \mathrm{T}\exp\left[\mathrm{i}g\int \mathrm{d}x^+\, A^-(x)\right]. \tag{39}$$

Effective action (38) includes the standard Yang–Mills term S_YM, as well as a gauge invariant generalization of the Abelian eikonal vertex $\int \mathrm{d}^4x\, \rho_a A_a^-$.[7]

At the tree level, $A_a^\mu \approx \mathcal{A}_a^\mu = \delta^{\mu i}\mathcal{A}_a^i$, where $\mathcal{A}_a^i$ is a solution of the classical equations of motion with the source ρ_a described in Section 2.2. The full gluon field in (36) and (37) includes both classical and quantum components:

$$A_a^\mu(x) \;=\; \mathcal{A}_a^\mu(x) + \delta A_a^\mu(x). \tag{40}$$

The mean field $\langle A_a^\mu(x)\rangle$ includes $\mathcal{A}^\mu$ and the contribution induced by quantum fluctuations $\langle \delta A^\mu\rangle$ corresponding to the polarization of gluon fluctuations by the external charge,

$$\langle A_a^\mu(x)\rangle = \mathcal{A}_a^\mu(x) + \langle \delta A_a^\mu(x)\rangle \equiv \mathcal{A}_a^\mu(x) + \delta\mathcal{A}_a^\mu(x), \tag{41}$$

and satisfies

$$\left\langle \frac{\delta S}{\delta A_a^\mu(x)}\right\rangle = 0 \tag{42}$$

(the brackets denote quantum averaging at fixed ρ).

Using generating functional (36), we can compute arbitrary gluon correlators. For example, the two-point correlator is given by

$$\langle\langle \mathrm{T}\, A^\mu(x)A^\nu(y)\rangle\rangle = \int \mathcal{D}\rho\, W_\Lambda[\rho]\, \frac{\int^\Lambda \mathcal{D}A\, A^\mu(x)A^\nu(y)\exp\left(\mathrm{i}S[A,\rho]\right)}{\int^\Lambda \mathcal{D}A\, \exp\left(\mathrm{i}S[A,\rho]\right)} \tag{43}$$

(double brackets indicate averaging with respect to both quantum fluctuations and the external source).

The sought effective theory can be constructed by layer-by-layer integration of quantum fluctuations with respect to p^+ (or p^-). The dominant contributions at small x are those proportional to large rapidity intervals $\Delta\tau = \ln(1/x) \gg 1$. We see in what follows that integration over p^+ in the strip $k^+ \ll p^+ \ll \Lambda^+$ generates corrections of the order $\alpha_\mathrm{s}\ln(\Lambda^+/k^+)$ to amplitudes with external momenta $k^+ < \Lambda^+$, which are essential if $\Lambda^+ \gg k^+$. From the standpoint of a more general description that takes quantum corrections into account, the MV model describes tree-level correlations of gluon fields where all degrees of freedom with longitudinal momenta larger than p^+ are already integrated out and the corresponding induced contributions are taken into account in the correspondingly renormalized parameters of the action. Summation of the logarithmic corrections is described in terms of a quantum evolution of the weight functional $W_\Lambda[\rho]$, where $\Lambda^+ \sim k^+$. The resulting classical theory is valid for modes with longitudinal momenta of the order of k^+.

3.2 Linear evolution: the Balitsky–Fadin–Kuraev–Lipatov limit

The evolution of the unintegrated structure function $\varphi(x,k_\perp^2)$ with a change in energy in the LLA in energy and lowest order in density is given by the BFKL equation [15]

$$\frac{\partial\varphi(\tau,k_\perp^2)}{\partial\tau} = \frac{\alpha_\mathrm{s}N_\mathrm{c}}{\pi^2}\int \mathrm{d}^2p_\perp\, \frac{k_\perp^2}{p_\perp^2(k_\perp-p_\perp)^2}\,\varphi(\tau,p_\perp^2) - \frac{1}{2}\,\frac{\alpha_\mathrm{s}N_\mathrm{c}}{\pi^2}\int \mathrm{d}^2p_\perp\, \frac{k_\perp^2}{p_\perp^2(k_\perp-p_\perp)^2}\,\varphi(\tau,k_\perp^2). \tag{44}$$

A key feature of BFKL equation (44) is the exponential growth of its solution with τ,

$$\varphi(\tau\to\infty) \sim \exp\left(c_\mathrm{BFKL}\tau\right), \tag{45}$$

where $c_\mathrm{BFKL} = \alpha_\mathrm{s}N_\mathrm{c}4\ln 2/\pi$. The asymptotics of form (45) means that the physical cross sections calculated in the linear approximation in the gluon density have a power-like divergence in the high-energy limit ($\tau = \ln 1/x \sim \ln\sqrt{s}$) and, thereby, violate unitarity. We note that the BFKL equation can be written not only for the unintegrated structure function but also, e.g., for the scattering amplitude of a fast color dipole on the target $\mathcal{N}(x_\perp,y_\perp)$, where $x_\perp$, $y_\perp$ are coordinates of the charges constituting the dipole in the transverse plane (see, e.g., Ref. [2]):

$$\frac{\partial\mathcal{N}(x_\perp,y_\perp)}{\partial\tau} = -\frac{\alpha_\mathrm{s}}{\pi}\int \mathrm{d}^2z_\perp\, \frac{(x_\perp-y_\perp)^2}{(x_\perp-z_\perp)^2(y_\perp-z_\perp)^2} \times \left[\mathcal{N}(x_\perp,z_\perp) + \mathcal{N}(z_\perp,y_\perp) - \mathcal{N}(x_\perp,y_\perp)\right]_\tau. \tag{46}$$

We stress once again that the linear approximation in the gluon density described in this subsection is conceptually unsatisfactory and needs improvement. A natural way to such an improvement is to work out a consistent nonlinear generalization of the linear formalism. We follow this logical line below.

3.3 Nonlinear evolution equation

To describe a quantum evolution of the weight functional $W_\Lambda[\rho]$ with Λ^+, it is convenient to consider two theories,

[6] We note that in the light-cone gauge, the 'longitudinal' separation of degrees of freedom is defined uniquely: the residual gauge transformations are independent of x^- and, therefore, cannot change the longitudinal momentum p^+.

[7] Strictly speaking, because of the nonlocal dependence of the eikonal interaction of the source ρ with A^- on time, the effective action should be considered on a contour in the complex plane. It can be shown, however, that in the LLA, one can restrict oneself to considering the dynamics on the real-time axis [28].

'Theory I' and 'Theory II', differing by their respective longitudinal scales Λ^+ and $b\Lambda^+$, where $b \ll 1$, but $\alpha_s \ln(1/b) < 1$. In Theory II, the modes in the strip

$$b\Lambda^+ < |p^+| < \Lambda^+ \tag{47}$$

separating Theories I and II are integrated out, and the induced contributions resulting from this integration are taken into account in the weight functional $W_{b\Lambda}$ by a suitable renormalization of its coefficients.

3.3.1 Nonlinear evolution equation: derivation. To explicitly calculate $\Delta W \equiv W_{b\Lambda} - W_\Lambda$, it is useful to compare the expressions for gluon correlators calculated at the same scale $k^+ \lesssim b\Lambda^+$ in the two theories. In Theory II, in the leading order in α_s, induced effects are taken into account at the tree level by definition. In Theory I, one has logarithmically amplified contributions from quantum fluctuations in strip (47). In computing quantum corrections, we keep the terms of the leading order in $\alpha_s \ln(1/b)$ (leading logarithmic approximation) to all orders in background fields and sources. This is necessary because of the key role of strong fields $\mathcal{A}^i \sim 1/g$ and sources $\rho \sim 1/g$ in our problem. The resulting equation [32, 35] is a nonlinear functional equation for $W_\tau[\rho]$ [here $\tau \equiv \ln(1/b)$] describing the evolution of $W_\tau[\rho]$ with growing τ.

We schematically consider calculations in Theory I in the example of the two-point equal time correlator $\langle A_a^i(x^+, \mathbf{k})\, A_a^i(x^+, -\mathbf{k})\rangle$ or, more precisely, its coordinate counterpart $\mathcal{G}(\mathbf{x}, \mathbf{y}) \equiv \langle A_a^i(x^+, \mathbf{x})\, A_a^i(x^+, \mathbf{y})\rangle$, which is, in fact, independent of x^+ because of the static nature of the source. In what follows, it is convenient to decompose the full gluon field as

$$A_a^\mu(x) = \mathcal{A}_a^\mu(x) + \delta A_a^\mu(x) + a_a^\mu(x)\,, \tag{48}$$

where $\mathcal{A}_a^\mu(x)$ is a classical solution, $\delta A_a^\mu(x)$ are the semihard quantum fluctuations with longitudinal momenta in the strip (47), and $a_a^\mu(x)$ are soft fields. Quantum effects important for our calculation arise from the interaction of soft modes a^μ with the semihard ones δA^μ in the presence of the external field $\mathcal{A}^i$ and the source ρ. A detailed analysis [28, 30] shows that in the LLA, $\delta\mathcal{A}^i \sim \alpha_s \log(1/b)\mathcal{A}^i$ and $\langle a^i a^i\rangle \sim \alpha_s \log(1/b)\mathcal{A}^i\mathcal{A}^i$, and therefore

$$\mathcal{G}(\mathbf{x}, \mathbf{y}) = \mathcal{A}^i(\mathbf{x})\,\mathcal{A}^i(\mathbf{y}) + \mathcal{A}^i(\mathbf{x})\,\delta\mathcal{A}^i(\mathbf{y}) + \delta\mathcal{A}^i(\mathbf{x})\,\mathcal{A}^i(\mathbf{y}) + \langle a^i(x^+, \mathbf{x})\, a^i(x^+, \mathbf{y})\rangle\,. \tag{49}$$

Correlator (49) contains three principal contributions: the tree-level one, the induced mean field, and the induced density corresponding to gluon polarization in the presence of the external source. The smallness of contributions nonlinear in a^i is due to the smallness of the induced fields compared to background ones. Because $\mathcal{A}^i$ and ρ are static, the induced mean field $\delta\mathcal{A}^i$ is also static, and the two-point functions, such as $\langle a_x^i a_y^j\rangle$, depend only on $x^+ - y^+$. We also note that $\langle\delta A^\mu\rangle = 0$.

As mentioned above, in calculating $\delta\mathcal{A}^i$ and $\langle\delta A^i\,\delta A^i\rangle$, we look at quantum contributions coming from semihard gluons. We note that the LLA imposes stringent restrictions on the kinematical definition of the semihard modes — these are the near-mass-shell modes with longitudinal momenta $b\Lambda^+ \ll |p^+| \ll \Lambda^+$ and frequencies $\Lambda^- \ll |p^-| \ll \Lambda^-/b$, where

$$\Lambda^- \equiv \frac{Q_\perp^2}{2\Lambda^+}\,, \tag{50}$$

and $Q_\perp$ is some characteristic transverse momentum.

The calculation aims at expressing $\delta\mathcal{A}^i$ and $\langle a^i a^i\rangle$ through correlators of the semihard modes in the LLA in $\alpha_s \ln(1/b)$ in the one-loop approximation. It turns out [35] that in the considered LLA, the sought logarithmic amplification is related to the correlator of the fluctuations of the charge density

$$\hat\chi_{ab}(x, y) \equiv \langle\delta\rho_a(x)\,\delta\rho_b(y)\rangle \tag{51}$$

and induced density

$$\hat\sigma_a(\mathbf{x}) \equiv \langle\delta\rho_a(x)\rangle = O\left(\alpha_s \ln\frac{1}{b}\,\rho\right). \tag{52}$$

It is convenient to isolate the logarithmic factor in (51) and (52) explicitly,

$$\hat\sigma_a(\mathbf{x}) \to \delta(x^-)\,\alpha_s \ln\frac{1}{b}\,\sigma_a(x_\perp) \equiv \delta(x^-)\int \mathrm{d}x^-\,\hat\sigma_a(x^-, x_\perp) \tag{53}$$

and

$$\hat\chi_{ab}(\mathbf{x}, \mathbf{y}) \to \delta(x^-)\,\alpha_s \ln\frac{1}{b}\,\chi_{ab}(x_\perp, y_\perp)\,\delta(y^-) \equiv \delta(x^-)\delta(y^-)\int \mathrm{d}x^- \int \mathrm{d}y^-\,\hat\chi_{ab}(\mathbf{x}, \mathbf{y})\,. \tag{54}$$

Correlator (49) then takes the form

$$\mathcal{G}(\mathbf{x}, \mathbf{y}) \approx \mathcal{A}_\mathbf{x}^i\mathcal{A}_\mathbf{y}^i + \alpha_s \ln\frac{1}{b}\left[(G^{iv}\mathcal{J}_v)_\mathbf{x}\,\mathcal{A}_\mathbf{y}^i + \mathcal{A}_\mathbf{x}^i(G^{iv}\mathcal{J}_v)_\mathbf{y} + (G^{i-}\chi\,G^{-i})_\mathbf{xy}\right]. \tag{55}$$

In expression (55), the virtual kernel σ is contained in $\mathcal{J}_v$. After averaging over ρ with the weight functional $W_\Lambda[\rho]$, formula (55) describes the gluon density at the scale $b\Lambda^+$ calculated to the LLA accuracy in Theory I.

The kernels σ and χ were calculated analytically in Refs [1, 27, 28, 30]. The result appears to depend on technical assumptions made in the calculations in Refs [27] and [1, 28, 30] (see also Ref. [33]). That the form of nonlinear terms in QCD evolution equations depends, in particular, on the way one fixes the residual gauge freedom is, in fact, not new (see, e.g., Ref. [17]).

We consider the same gluon correlator (49) in Theory II. By construction,

$$\langle\mathcal{A}_\mathbf{x}^i\mathcal{A}_\mathbf{y}^i\rangle_{b\Lambda} = \langle\mathcal{A}_\mathbf{x}^i\mathcal{A}_\mathbf{y}^i\rangle_\Lambda + \alpha_s \ln\frac{1}{b}\left\langle(G^{iv}\mathcal{J}_v)_\mathbf{x}\,\mathcal{A}_\mathbf{y}^i + \mathcal{A}_\mathbf{x}^i(G^{iv}\mathcal{J}_v)_\mathbf{y} + (G^{i-}\chi\,G^{-i})_\mathbf{xy}\right\rangle_\Lambda, \tag{56}$$

where

$$\langle\mathcal{A}_\mathbf{x}^i\mathcal{A}_\mathbf{y}^i\rangle_\Lambda \equiv \int \mathcal{D}\rho\, W_\Lambda[\rho]\,\mathcal{A}_a^i(\mathbf{x})\,\mathcal{A}_a^i(\mathbf{y})\,. \tag{57}$$

Analogous formulas can be written for $\langle\mathcal{A}^i\mathcal{A}^i\rangle_{b\Lambda}$ in terms of $W_{b\Lambda}$. Equation (56) is, in fact, an evolution equation for the

gluon density that can be used for the derivation of the evolution equation for the weight functional $W_\Lambda[\rho] \to W_{b\Lambda}[\rho]$.

The derivation is performed in two stages. At the first stage, one shows that the expressions for quantum corrections can be reproduced by adding a Gaussian random source to the right-hand side of classical equations of motion (2), and at the second stage, one performs the necessary redefinitions of the classical source and the weight functional.

In more detail, one considers the modified equations of motion

$$[\mathrm{D}_\nu, F^{\nu\mu}]_a = \delta^{\mu+}\big(\rho_a(\mathbf{x}) + v_a(\mathbf{x})\big)\,, \tag{58}$$

with the random source $v_a(\mathbf{x})$ chosen such that on solutions of Eqn (58), with quantum corrections taken into account, the correlator $\langle A^i A^i\rangle$ coincides with that calculated in Theory I. The noise v_a thus plays the role of fluctuations in the charge density $\delta\rho_a$ induced by the semihard modes. Using this analogy, one assumes that v_a is stationary and has the same correlators as $\delta\rho_a$,

$$\big\langle v_a(\mathbf{x})\big\rangle_v = \sigma_a(\mathbf{x})\,, \qquad \big\langle v_a(\mathbf{x})\, v_b(\mathbf{y})\big\rangle_v = \chi_{ab}(\mathbf{x},\mathbf{y})\,, \tag{59}$$

where the brackets $\langle\ldots\rangle_v$ denote averaging over v.

A simple analysis shows [28, 30] that correlators calculated in Theories I and II coincide if the wave functional W satisfies the quadratic relation

$$\int \mathcal{D}\rho\, W_{b\Lambda}[\rho]\, \mathcal{A}^i_x[\rho]\, \mathcal{A}^i_y[\rho] = \int \mathcal{D}\rho\, W_\Lambda[\rho] \int \mathcal{D}v\, W[v\,;\rho]\, \mathcal{A}^i_x[\rho+v]\, \mathcal{A}^i_y[\rho+v]\,. \tag{60}$$

Expanding the integrand in the right-hand-side of (60) up to the second order in $v\delta/\delta\rho$ and integrating over v, one obtains the relation for the integrands in (60):

$$W_{b\Lambda}[\rho] - W_\Lambda[\rho] = -\frac{\delta}{\delta\rho_x}\,[W_\Lambda\sigma_x] + \frac{1}{2}\,\frac{\delta^2}{\delta\rho_x\,\delta\rho_y}\,[W_\Lambda\chi_{xy}]\,. \tag{61}$$

We stress that convolutions on the right-hand-side of (61) contain three-dimensional integration, e.g.,

$$\frac{\delta}{\delta\rho_x}\,[W_\Lambda\sigma_x] \equiv \int \mathrm{d}^3\mathbf{x}\,\frac{\delta}{\delta\rho_a(\mathbf{x})}\,\big[W_\Lambda\sigma_a(\mathbf{x})\big]\,. \tag{62}$$

We also note that because the support of σ lies in the interval $1/\Lambda^+ \lesssim x^- \lesssim 1/b\Lambda^+$, the logarithmic amplification arises only after the integration over x^-. In the limit as $b \to 1$, equality (62) can be transformed into

$$\frac{\delta}{\delta\rho_x}\,[W_\Lambda\sigma_x] = \alpha_\mathrm{s}\ln\frac{1}{b}\int \mathrm{d}^2x_\perp\,\frac{\delta}{\delta\rho_a(x^-_\Lambda, x_\perp)}\,\big[W_\Lambda\sigma_a(x_\perp)\big]\,. \tag{63}$$

In terms of rapidity, $\tau \equiv \ln(P^+/\Lambda^+) = \ln(1/x)$, and hence $\ln(P^+/b\Lambda^+) = \tau + \Delta\tau$, where $\Delta\tau \equiv \ln(1/b)$. After evident notation changes $W_\Lambda \equiv W_\tau$, $W_{b\Lambda} \equiv W_{\tau+\Delta\tau}$, and $x^-_\Lambda = 1/\Lambda^+ \equiv x^-_\tau$, relation (61) becomes

$$W_{\tau+\Delta\tau}[\rho] - W_\tau[\rho] = \alpha_\mathrm{s}\Delta\tau\left\{\frac{1}{2}\,\frac{\delta^2}{\delta\rho_\tau(x)\,\delta\rho_\tau(y)}\,[W_\tau\chi_{xy}] - \frac{\delta}{\delta\rho_\tau(x)}\,[W_\tau\sigma_x]\right\}, \tag{64}$$

where $\rho_\tau(x_\perp) \equiv \rho(x^-_\tau, x_\perp)$ and the convolutions are understood as two-dimensional integrals, e.g.,

$$\frac{\delta}{\delta\rho_\tau(x)}\,[W_\tau\sigma_x] = \int \mathrm{d}^2x_\perp\,\frac{\delta}{\delta\rho_a(x^-_\tau, x_\perp)}\,\big[W_\tau\sigma_a(x_\perp)\big]\,. \tag{65}$$

According to (64) and (65), the evolution from $W_\tau[\rho]$ to $W_{\tau+\Delta\tau}[\rho]$ is generated by the changes in the source ρ in the interval of rapidities $(\tau, \tau+\Delta\tau)$ in which, in the LLA used, quantum corrections are essential.[8] We note that the coordinate support of the source correlates with the longitudinal momenta of the modes over which the integration is performed. Therefore, the rapidity τ can be interpreted both as a momentum, $\tau = \ln(P^+/\Lambda^+)$, and as a coordinate $\tau = \ln(x^-_\tau/x^-_0)$ (here, x^-_0 is some arbitrary longitudinal scale, e.g., $x^-_0 = 1/P^+$).

Taking the limit as $\Delta\tau \equiv \ln(1/b) \to 0$ yields the final equation describing the evolution of the wave functional in $\tau \equiv \ln(1/x)$, first obtained via direct computation in Ref. [35],

$$\frac{\partial W_\tau[\rho]}{\partial\tau} = \alpha_\mathrm{s}\left\{\frac{1}{2}\,\frac{\delta^2}{\delta\rho_\tau(x)\,\delta\rho_\tau(y)}\,[W_\tau\chi_{xy}] - \frac{\delta}{\delta\rho_\tau(x)}\,[W_\tau\sigma_x]\right\}. \tag{66}$$

Equation (66) is a functional Fokker–Planck equation, in which τ plays the role of time, describing diffusion in the space of charge densities ρ with ρ-dependent drift and diffusion coefficients $\alpha_\mathrm{s}\sigma$ and $\alpha_\mathrm{s}\chi$. In the language of random processes, Eqn (60) is a Chapman–Kolmogorov equation. Equation (66) can also be interpreted as a functional Schrödinger equation in the imaginary time τ. Evolution equation (66) leads to a chain of evolution equations for the charge density correlators $\langle\rho\rho\ldots\rho\rangle_\tau$ [35]. In particular, multiplying $W_\tau[\rho]$ by $\rho(x)\,\rho(y)$ and performing the functional integration over ρ, we obtain an evolution equation for the two-point correlator,

$$\frac{\mathrm{d}}{\mathrm{d}\tau}\big\langle\rho_a(\mathbf{x})\,\rho_b(\mathbf{y})\big\rangle_\tau = \alpha_\mathrm{s}\big\langle\delta(x^- - x^-_\tau)\,\sigma_a(x_\perp)\,\rho_b(\mathbf{y}) + \delta(y^- - x^-_\tau)\,\rho_a(\mathbf{x})\,\sigma_b(y_\perp) + \delta(x^- - x^-_\tau)\,\delta(y^- - x^-_\tau)\,\chi_{ab}(x_\perp, y_\perp)\big\rangle_\tau\,, \tag{67}$$

where $\langle\ldots\rangle_\tau$ denotes averaging over ρ with the weight functional $W_\tau[\rho]$.

3.3.2 Nonlinear evolution equation: α-representation. All physically interesting correlators can be computed in terms of tree-level correlators of color charge density and the quantum corrections to them. At the same time, a more transparent picture of quantum evolution arises in the covariant gauge if all correlators are expressed through the background field α introduced in Section 2.2. The new evolution equation is given by [29, 30]

$$\frac{\partial W_\tau[\alpha]}{\partial\tau} = \alpha_\mathrm{s}\left\{\frac{1}{2}\,\frac{\delta^2}{\delta\alpha_\tau(x)\,\delta\alpha_\tau(y)}\,[W_\tau\eta_{xy}] - \frac{\delta}{\delta\alpha_\tau(x)}\,[W_\tau v_x]\right\}. \tag{68}$$

Evolution equation (68) involves new virtual and real kernels v and η. Explicit computations [29, 30] lead to the following

[8] A detailed discussion can be found in Ref. [37].

simple expressions for them:

$$v^a(x_\perp) = \frac{ig}{2\pi}\int \frac{d^2z_\perp}{(2\pi)^2}\,\frac{1}{(x_\perp - z_\perp)^2}\,\mathrm{Tr}\left(T^a\Omega^\dagger(x_\perp)\,\Omega(z_\perp)\right),$$

$$\eta^{ab}_{x_\perp,y_\perp} = \frac{1}{\pi}\int \frac{d^2z_\perp}{(2\pi)^2}\,\frac{(x^i - z^i)(y^i - z^i)}{(x_\perp - z_\perp)^2(y_\perp - z_\perp)^2} \times\left\{1 + \Omega^\dagger(x_\perp)\,\Omega(y_\perp) - \Omega^\dagger(x_\perp)\,\Omega(z_\perp) - \Omega^\dagger(z_\perp)\,\Omega(y_\perp)\right\}^{ab}. \tag{69}$$

Here, T_a is a generator of SU(N) in the adjoint representation.

Using the α-representation allows, in particular, constructing a neat Hamiltonian form of evolution equation (68) first obtained by Weigert [94]. In more detail, an explicit calculation shows [94] that there exists a remarkable equation interrelating the coefficients of evolution equation (68) (and, therefore, real and virtual contributions),

$$\frac{1}{2}\int d^2y_\perp\,\frac{\delta\eta^{ab}(x_\perp,y_\perp)}{\delta\alpha^b(y_\perp)} = v^a(x_\perp), \tag{70}$$

which allows rewriting evolution equation (68) in the Hamiltonian form:

$$\frac{\partial W_\tau[\alpha]}{\partial\tau} = \left\{\int\frac{d^2z_\perp}{2\pi}\,J^i_a(z_\perp)\,J^i_a(z_\perp)\right\}W_\tau[\alpha] \equiv -HW_\tau[\alpha], \tag{71}$$

$$J^i_a(z_\perp) = i\int\frac{d^2x_\perp}{2\pi}\,\frac{z^i - x^i}{(z_\perp - x_\perp)^2}\left[1 - \Omega^\dagger(z_\perp)\,\Omega(x_\perp)\right]_{ab}\frac{\delta}{\delta\alpha^b_\tau(x_\perp)}.$$

In discussing solutions of nonlinear renormalization group equation (68) or its Hamiltonian analogue (71), a diligent analysis of the structure of functional derivatives with respect to α is required [30, 43] (see also Ref. [95]). The main idea is that, as follows from the experience in computing quantum corrections to the MV model, the development of quantum evolution up to the scale τ generates the field α with support in the interval $0 \leqslant x^- \leqslant \exp(\tau)/P^+ \equiv x_0^-\exp(\tau) \equiv x_\tau^-$. Within the considered RG procedure, one can then make the replacement

$$\Omega^\dagger(x_\perp) \to \Omega^\dagger_\tau(x_\perp) \equiv \mathrm{P}\exp\left\{ig\int_0^{x_\tau^-} dx^-\,\alpha(x^-,x_\perp)\right\}. \tag{72}$$

Detailed analysis shows [30] that quantum evolution (i.e., the changes in the tree-level field configuration induced by quantum corrections) occurs at the boundary of the tree-level source in the coordinate x^- such that the derivatives of Wilson lines (72) in renormalization group equations (68) and (71) are in fact taken with respect to the colored field $\alpha_\tau(x_\perp) \equiv \alpha(x_\tau^-, x_\perp)$ at the endpoint x_τ^-:

$$\frac{\delta\Omega^\dagger_\tau(x_\perp)}{\delta\alpha^a_\tau(z_\perp)} = ig\delta^{(2)}(x_\perp - z_\perp)\,T^a\Omega^\dagger_\tau(x_\perp). \tag{73}$$

It is very important to take this circumstance into account when discussing the general properties of solutions of master equations (66) and (68) and their physical interpretation [43–45]. In particular, the quantities $\Omega_\tau(x_\perp)$ and their canonically conjugate momenta

$$\Pi^a_\tau(x_\perp) = \frac{1}{ig}\,\frac{\delta}{\delta\alpha^a_\tau(x_\perp)} \tag{74}$$

are the true canonical variables of the theory [30].

As already mentioned, evolution equations (68) allow calculating an arbitrary correlator of α-dependent operators. The evolution equation for one of the functionals of α that is of special interest, namely, for $\mathcal{V}(x_\perp,y_\perp) \equiv \mathrm{Tr}\left(\Omega^\dagger(x_\perp)\,\Omega(y_\perp)\right)$, has the form [30]

$$\frac{\partial\mathcal{V}(x_\perp,y_\perp)}{\partial\tau} = -\frac{\alpha_s}{2\pi^2}\int d^2z_\perp\,\frac{(x_\perp - y_\perp)^2}{(x_\perp - z_\perp)^2(y_\perp - z_\perp)^2} \times\left\langle N_c\mathcal{V}(x_\perp,y_\perp) - \mathcal{V}(x_\perp,z_\perp)\,\mathcal{V}(z_\perp,y_\perp)\right\rangle_\tau. \tag{75}$$

Equation (75) was first derived by Balitsky [40] using the formalism of the functional operator expansion on the light cone.

3.3.3 Nonlinear evolution equation: results. Before turning to a description of the known (approximate) analytical solutions of (68), we discuss a simple closure of the hierarchy of Eqns (75) reducing all higher order correlators to the products of basic two-point functions, e.g.,

$$\left\langle\mathcal{V}(x_\perp,z_\perp)\,\mathcal{V}(z_\perp,y_\perp)\right\rangle_\tau \to \left\langle\mathcal{V}(x_\perp,z_\perp)\right\rangle_\tau\left\langle\mathcal{V}(z_\perp,y_\perp)\right\rangle_\tau.$$

Such factorization arises 'automatically' in the limit of large N_c. The above-introduced combination $\mathcal{V}(x_\perp,y_\perp)$ is related to the scattering amplitude $\mathcal{N}(r_\perp \equiv x_\perp - y_\perp)$ of a corresponding (dependent on the representation of the gauge group used in constructing a Wilson line) color dipole:

$$\mathcal{N}(r_\perp) = \frac{1}{N_c}\left[\mathrm{Tr}\,(1) - \mathcal{V}(x_\perp,y_\perp)\right]. \tag{76}$$

The corresponding evolution equation for $\mathcal{N}$, first derived by Balitsky [40], has the form

$$\frac{\partial\mathcal{N}(x_\perp,y_\perp)}{\partial\tau} = -\frac{\alpha_s}{\pi}\int d^2z_\perp\,\frac{(x_\perp - y_\perp)^2}{(x_\perp - z_\perp)^2(y_\perp - z_\perp)^2} \times\left[\mathcal{N}(x_\perp,z_\perp) + \mathcal{N}(z_\perp,y_\perp) - \mathcal{N}(x_\perp,y_\perp) - \mathcal{N}(x_\perp,z_\perp)\,\mathcal{N}(z_\perp,y_\perp)\right]_\tau. \tag{77}$$

Equation (77) was independently derived by Kovchegov [41] in the framework of the color dipole model formalism and subsequently rederived in Ref. [96] by direct resummation of the contributions of triple-pomeron vertices. Recently, a derivation of this equation within the reggeon formalism was given [22]. It is important to note that by its physical meaning, $\mathcal{N}(x_\perp,y_\perp)$ is a scattering amplitude *at a fixed impact parameter* $b_\perp = (x_\perp + y_\perp)/2$, $\mathcal{N}(x_\perp,y_\perp) \equiv \mathcal{N}(b_\perp,r_\perp)$, where $r_\perp = x_\perp - y_\perp$. This circumstance is of importance for us in discussing the interrelation between saturation and unitarity in Section 3.4.

The properties of the solution of (77) are best illustrated by its convenient parameterization proposed in Ref. [97]:

$$\mathcal{N}(x_\perp,y_\perp) = 1 - \exp\left[-(r_\perp)^2\,Q_s^2(\tau,b_\perp)\right]. \tag{78}$$

In Eqn (78), the dependence of the scattering amplitude $\mathcal{N}$ on the energy is controlled by the dependence of the saturation momentum Q_s^2 on τ. An intensive analytical and numerical analysis [42, 43, 46, 56] has shown that the following simple parameterization of the dependence of the saturation scale $Q_s(b_\perp,\tau)$ on energy is valid:

$$Q_s^2(\tau,b_\perp) = Q_s^2(\tau_0,b_\perp)\exp\left[c\alpha_s(\tau - \tau_0)\right], \tag{79}$$

where c is a numerical coefficient, $c \sim 1$. From Eqns (78) and (79), we see that the magnitude of the scattering amplitude is determined by a multiplicative combination of the probe size $Q_\perp^2 \sim 1/r_\perp^2$ and rapidity τ. At large $Q_\perp^2$ and moderate τ, we obtain the standard perturbative answer $\mathcal{N} \sim 1/Q_\perp^2$. Most interesting is, of course, the high-energy limit $\tau \to \infty$ in which, due to $\bar{Q}_s^2(\tau \to \infty) \to \infty$ [cf. (79)], the second term in (78) equals zero and the scattering amplitude is saturated at its upper limit, $\mathcal{N}(\tau \to \infty) \to 1$. Therefore, the quadratic nonlinearity of Balitsky–Kovchegov equation (77) ensures unitarization *at a fixed impact parameter* $b_\perp$. Transition from the purely perturbative regime at intermediate energies to the nonlinear regime at high energies is controlled by the key parameter of the theory, the saturation scale.

Is it possible to give a compact description of the theory in the whole range of transverse momenta? In Ref. [45], it was shown, in particular, that due to completely different reasons, the asymptotics at both small ($q_\perp^2 \ll Q_s^2$) and large ($q_\perp^2 \gg Q_s^2$) transverse momenta are described by the Gaussian weight functional W satisfying the equation

$$\frac{\partial W_\tau[\rho]}{\partial \tau} = \frac{1}{2} \int \mathrm{d}^2 x_\perp \, \mathrm{d}^2 y_\perp \, \lambda(x_\perp, y_\perp) \, \frac{\delta^2 W_\tau[\rho]}{\delta \rho_\tau^a(x_\perp) \, \delta \rho_\tau^a(y_\perp)} \,. \quad (80)$$

At large transverse momenta, one can simply neglect all nonlinear effects, and a complete description of the system is provided by the two-point function satisfying the BFKL equation. At small transverse momenta, the situation is again Gaussian, but this time because of the nonlinearities in the equation kernel being small due to oscillations of the arguments of the Wilson lines in it. It turns out that with good accuracy the solution of the general master equation (66) or (68) can be approximated by the Gaussian satisfying Eqn (80) with the kernel interpolating between the regimes of small and large transverse momenta:

$$\lambda_\tau(k_\perp) = \lambda_\tau^{\mathrm{BFKL}} \, \frac{k_\perp^2}{k_\perp^2 + \pi \lambda_\tau^{\mathrm{BFKL}}} \,. \quad (81)$$

We also mention an important observation made in Refs [43, 44], namely, a 'geometrical scaling' of the kernel

$$\lambda_\tau(k_\perp) \simeq \frac{1}{\pi} \, k_\perp^2 \left(\frac{Q_s^2(\tau)}{k_\perp^2} \right)^\gamma \quad (82)$$

(γ is some constant) valid in the 'scaling window' $Q_s^2(\tau) \ll k_\perp^2 \ll Q_s^4(\tau)/Q_0^2$ and leading to the corresponding scaling behavior of physical observables.

In concluding this section, we also mention recent papers [47, 48] analyzing the distinctions in the solutions of the full renormalization group evolution equation and its simplified variant, the Balitsky–Kovchegov evolution equation.

3.4 Saturation and unitarity

Equation (78) demonstrates the saturation phenomenon in terms of the dipole scattering amplitude. Indeed, it follows from Eqn (78) that the scattering amplitude for large dipoles (i.e., those for which the distance between the charges in the transverse plane $r_\perp^2 \equiv (x_\perp - y_\perp)^2 > Q_s^2$) is small. We note once again that the right-hand side of Eqn (78) depends only on the dipole size $r_\perp \equiv x_\perp - y_\perp$, and hence the equation is valid at a *fixed* impact parameter $b \equiv (x_\perp + y_\perp)/2$. Unitarity (e.g., meeting the condition $N \leqslant 1$) is thus ensured at fixed b only.

At this stage, the most important question to answer is whether saturation also helps to solve the unitarity violation problem for the full inelastic cross section, obtained by integrating the scattering amplitude over the impact parameter. Unfortunately, the answer to this question turns out to be negative. A detailed analysis of the problem is given in Refs [50–53].

The unitarity requirement in the theory leads to the famous Froissart bound on the maximally allowed growth of the total inelastic cross section with collision energy E,

$$\sigma_{\mathrm{inel}} < \frac{\pi}{m_\pi^2} \, (\ln E)^2 \equiv \frac{\pi}{m_\pi^2} \, \tau^2 \,, \quad (83)$$

where m_π is the smallest mass in the theory (the pion mass in QCD with light quarks).

The physical cross section for the scattering of the probe, having the transverse size $Q_\perp^2 \sim 1/r_\perp^2$ at the energy $\sim \exp(\tau)$, is obtained by integrating the scattering amplitude $\mathcal{N}$ over the impact parameter $b_\perp$,

$$\sigma(Q_\perp^2, \tau) = 2 \int \mathrm{d}^2 b_\perp \, N(Q_\perp, b_\perp | \tau) \equiv \pi R^2(\tau) \,, \quad (84)$$

where we introduce an energy-dependent interaction radius $R(\tau)$. In terms of this radius, Froissart bound (83) corresponds to the maximally allowed growth of the interaction radius $R(\tau) \sim \tau$.

A key reason for the unitarity violation is easily understood by noticing that in perturbation theory, the behavior of the fields at spatial infinity for both colored and color-neutral systems is always power-like. Therefore, for sufficiently large impact parameters $b_\perp$ and sufficiently high energies, the integral in (84) has a power-like divergence. This effect can be characterized by a compact formula for the total cross section derived in Ref. [51],

$$\sigma_{\mathrm{inel}} = \pi R_{\mathrm{target}}^2 + 2\pi R_{\mathrm{target}} \, x_0 \exp\left(\frac{\alpha_s N_c}{2\pi} \epsilon \tau \right) , \quad (85)$$

where ϵ is a constant. We see from Eqn (85) that at large τ, the growth of the total cross section is exponential and thus violates the Froissart bound. One more point elucidating the reasons for unitarity violation is the impossibility of perturbative generation of mass in the non-Abelian massless gauge theory; the perturbation theory cannot generate the mass m_π [cf. (83)] that turns a power-like dependence of the scattering amplitude on the impact parameter into an exponential one and thus saves unitarity. Therefore, beyond nonlinear effects taken into account in the above-described modified perturbation theory, there remain many important nonperturbative phenomena having to do with the restoration of unitarity broken down in the perturbative description (a detailed discussion of these issues in terms of constituent quarks, the soft pomeron, etc. can be found in Ref. [52]).

4. Dense gluon matter in nuclear collisions

Of exceptional interest to the studies of non-Abelian parton dynamics are ultrarelativistic heavy-ion collisions, because the dense initial partonic fluxes are present in them and provide conditions for the creation of dense partonic matter at the early stages of these collisions.

To describe the parton-related dynamics of nuclear collisions at high energy, it is necessary to exactly specify the role of partonic degrees of freedom within the chosen description of nuclear interactions. Below, we discuss two approaches existing in the literature. [9]

In the first one, one considers [56, 62] a mixture of soft nonperturbative (e.g., hadronic strings) and semihard perturbative contributions to the inelastic cross section. The perturbative cross sections are strongly divergent at small momentum transfer (small transverse energy), and therefore, to arrange a finite contribution to the inelastic cross section, one has to introduce an explicit infrared cutoff. The dominant contribution to the perturbative component of the inelastic cross section therefore comes from the infrared cutoff scale — a situation that is not conceptually satisfactory (the infrared divergence of the perturbative cross sections is typically power-like, and therefore introducing a cutoff presents a 'brutal' way of fixing a physically important scale).

In the second approach [57, 68], related to the physical implications of the gluon saturation phenomenon, the saturation scale Q_s is not introduced artificially, but arises due to nonlinear effects in a dense gluon medium. Technically speaking, the saturation momentum Q_s plays the role of an infrared regulator, and the dominant contribution to the physical cross section is again coming precisely from the vicinity of this momentum scale. An important difference from the mixed type models is that in saturation type models, it is extremely difficult, if at all possible, to consistently add a soft nonperturbative component into consideration.

4.1 Mixed model

The most complete description of the dynamics of heavy-ion collisions based on superposition of soft stringy and semihard partonic dynamics currently available is provided by the HIJING model [62]. In addition to taking initial and final state radiation in hadronic collisions into account, the model also accounts for nuclear shadowing of the structure functions and the energy loss of produced partons in the debris created in a nuclear collision. The nuclear collision is described in HIJING as a superposition of nucleon – nucleon collisions. The hadronic p – p block of HIJING is 'normalized' on experimental data at the energies ~ 100 GeV, and hence, in this sense, the model is adequately tuned to RHIC energies. Although it is probably very difficult to extrapolate, without major modifications, the physics embedded into HIJING to the Large Hadron Collider (LHC) energies, at RHIC energies the model provides a sufficiently balanced and reliable basis for analyzing the physics of nuclear collisions.

A good illustration of the use of the mixed 'soft – hard' approach is the formula for the energy and centrality dependence of the (pseudo)rapidity particle density containing a characteristic mix of soft and hard contributions [86, 98],

$$\frac{\mathrm{d}N}{\mathrm{d}y} = \big(1 - X(s)\big)\, n_{\mathrm{p-p}}\, \frac{\langle N_{\mathrm{part}}\rangle}{2} + X(s)\, n_{\mathrm{p-p}} \langle N_{\mathrm{coll}}\rangle\,, \qquad (86)$$

where $n_{\mathrm{p-p}}$ is the pseudorapidity particle density in p – p collisions, $X(s)$ is the yield of semihard dynamics in particle production, and $\langle N_{\mathrm{part(coll)}}\rangle$ are the average numbers of participants (collisions) at a given energy. We recall that by 'participants', we understand the nucleons having experienced at least one inelastic collision, while the subscript 'coll' refers to counting all inelastic collisions. The estimate of $X(s)$ in Ref. [86] gave $X(130\ \mathrm{GeV}) \sim 0.1$, i.e., a ten percent share of semihard particle production mechanisms.

4.1.1 Anatomy of the transverse energy flow. Before turning to the analysis of nuclear collisions, we discuss the 'anatomy' of the transverse energy flow generated in multiparticle production processes in nucleon – nucleon interactions in terms of the relative contributions of various perturbative and nonperturbative mechanisms. As mentioned above, nucleon – nucleon collisions constitute a basic element in the construction of mixed type models like HIJING, and hence the results of this analysis will help to gauge, through comparison with experimental data [99], contributions to the observed transverse energy flow due to different mechanisms and give their physical interpretation.

We first turn to the calculation of the perturbative contribution to the transverse energy flow in the central rapidity window in the next-to-leading order (NLO) approximation and compare it to experimental data obtained by the UA2 collaboration [99]. In general, a calculation of the jet cross section to the NLO accuracy requires using a so-called jet-defining algorithm specifying the resolution for the jet to be observed, for example, the angular size of the jet-defining cone (see, e.g., Ref. [59]). The considered cross section is calculated by integrating the differential one over the phase space, with the integration domain restricted by the jet characteristics imposed by the jet-defining algorithm. The transverse energy distribution in a given rapidity interval $y_a < y < y_b$ in the NLO with an accuracy of $O(\alpha_s^3)$ is calculated from the formula

$$\begin{aligned}\frac{\mathrm{d}\sigma}{\mathrm{d}E_\perp} = {} & \int \mathrm{D}^2\mathrm{PS}\, \frac{\mathrm{d}\sigma}{\mathrm{d}^4 p_1\, \mathrm{d}^4 p_2} \\ & \times \delta\left[E_\perp - \sum_{i=1}^{2} |\, p_{\perp i}|\, \theta(y_{\min} < y_i < y_{\max})\right] \\ & + \int \mathrm{D}^3\mathrm{PS}\, \frac{\mathrm{d}\sigma}{\mathrm{d}^4 p_1\, \mathrm{d}^4 p_2\, \mathrm{d}^4 p_3} \\ & \times \delta\left[E_\perp - \sum_{i=1}^{3} |\, p_{\perp i}|\, \theta(y_{\min} < y_i < y_{\max})\right], \end{aligned} \qquad (87)$$

where $\mathrm{D}^{2(3)}\mathrm{PS}$ denotes integration over the two-dimensional (three-dimensional) phase space. The first contribution corresponds to the two-particle final state with one-loop radiative corrections taken into account, and the second one to the three-particle final states. In perturbative QCD, one can rigorously compute only infrared-safe quantities [59], in which the divergences related to real and virtual contributions compensate each other, such that adding one very soft gluon does not change the answer. It is easy to convince oneself that the transverse energy distribution into a given rapidity interval calculated with formula (87) satisfies the above requirement. [10]

The calculation of the transverse energy spectrum in p – $\bar{\mathrm{p}}$ collisions was performed in Ref. [64] using the Monte Carlo

[9] In the literature, an analysis of nuclear collision dynamics in terms of gluon strings stretching between constituent degrees of freedom is also discussed (see., e.g., Ref. [5]).

[10] For a formal definition of infrared safety, see, e.g., Ref. [100].

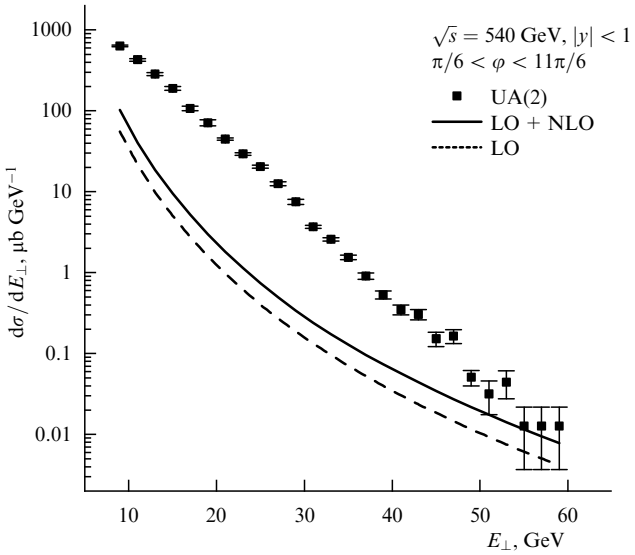

Figure 1. Transverse energy spectrum in $p-\bar{p}$ collisions: broken and solid lines are calculations to the LO and (LO + NLO) accuracy in perturbative QCD, respectively; squares are experimental data by the UA2 collaboration [99].

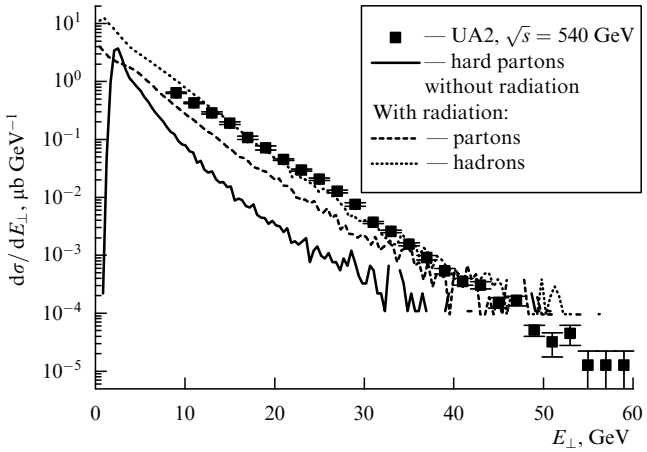

Figure 2. Transverse energy spectrum in $p-\bar{p}$ collisions calculated in HIJING compared with the experimental data by the UA2 collaboration [99].

code developed in Ref. [100] and a 'jet' definition corresponding to the studied transverse energy production spectrum (87).

In Fig. 1, we compare the LO and (LO + NLO) transverse energy spectra in $p-\bar{p}$ collisions calculated according to the method described in Ref. [60], with the experimental transverse energy distribution in the central rapidity window $|y| < 1$ and azimuthal coverage $\pi/6 \leqslant \varphi \leqslant 11\pi/6$ at $\sqrt{s} = 540$ GeV measured by the UA2 Collaboration [99]. We see that the perturbative LO + NLO calculations agree with experimental data only at large enough energies $E_\perp \gtrsim 60$ GeV. It is interesting to note that precisely around this energy, the space of experimental events becomes dominated by the two-jet configurations [99]. This means that only starting from these transverse energies do the assumptions on which perturbative calculations are based (collinear factorization in the leading twist, an explicit account for all contributions of a given order in α_s) allow describing the process of transverse energy production and ensuring the required duality between the description of dominant configurations contributing in the considered order in perturbation theory and the transverse energy carried by hadrons in the final state. At $E_\perp \leqslant 50$ GeV, the calculated spectrum is in radical disagreement with the experimental one both in shape and magnitude, demonstrating the inadequacy of the considered $O(\alpha_s^3)$ perturbative calculation in this domain. We note that it is currently impossible to improve the results of the above calculation, because neither calculations of the considered spectrum in higher orders nor infinite-order resummation of the corresponding perturbation theory series for this process have so far been performed.

In practical terms, this means that to achieve agreement with experimental data, one needs to invoke additional model assumptions that cannot be avoided when accounting for higher-order and higher-twist effects. In the popular Monte Carlo generators PYTHIA [65] and HIJING [62], the effects such as multiple binary parton–parton collisions, initial and final state radiation, and transverse energy production during hadronization are taken into account. In Fig. 2, we compare the same experimental data by UA(2) [99] with the spectrum calculated with the HIJING event generator. In Fig. 2, to illustrate the relative contribution of different dynamical mechanisms, we plot the contributions from hard parton scattering without initial and final state radiation, the full partonic contribution and, finally, the transverse energy spectrum of final hadrons. We see that taking additional partonic sources such as initial and final state radiation into account allows reproducing the (exponential) form of the spectrum, but still not the magnitude. The remaining gap is filled in by soft contributions due to transverse energy production from decaying stretched hadronic strings. We finally note that the spectrum calculated in HIJING is somewhat steeper than the experimental one. An additional fine tuning can be achieved by selecting different structure functions.

The described results clearly demonstrate that in order to reproduce the experimentally observed transverse energy spectrum, one has to invoke complicated mechanisms of parton production that account for radiation accompanying the hard parton–parton scattering in both the initial and final stages of this process, as well as production of gluonic kinks (collective excitations of the gluon strings) by these strings and the nonperturbative generation of transverse energy at the hadronization stage. This statement is a calorimetric analog of the well-known result on the importance of the minijet component in describing the tails of multiplicity distributions [62, 101].

We note that the above-described results have the most direct relation to the description of the early stages of heavy-ion collisions. In most dynamical models of nucleus–nucleus collisions, the description is made in terms of an incoherent superposition of nucleon–nucleon collisions. As we have convinced ourselves, to correctly describe the partonic configuration 'preceding' the observed transverse energy flow in nucleon–nucleon collisions, mechanisms beyond conventional collinear factorization have to be invoked. This means that to estimate such quantities as, e.g., parton multiplicity at some given time scale, a very careful analysis of various contributions is required.

4.1.2 Azimuthal pattern of transverse energy flow. To understand the parton-related dynamical features of heavy-ion

collisions, one needs to analyze the experimentally observable quantities sensitive to particular features, distinguishing semihard parton dynamics from the soft hadronic one. One specific proposal was discussed in Refs [64, 65]. The idea is that the perturbative mechanism generates an asymmetric flow of transverse energy due to its collimation along the directions fixed in the processes with large momentum transfer.

To quantify an event-by-event asymmetry of transverse energy flow, we consider the difference between the transverse energy deposited, in some rapidity window $y_{\min} < y_i < y_{\max}$, into two oppositely azimuthally oriented sectors with a specified angular opening $\delta\varphi$ each.

For convenience and without restricting the generality of the description, we can think of the directions of these cones as being 'up' or 'down' in some specially chosen coordinate system in the transverse plane. All results are, of course, insensitive to the particular choice. Denoting the transverse energy going into the 'upper' and 'lower' cones in a given event by $E_\perp^\uparrow(\delta\varphi)$ and $E_\perp^\downarrow(\delta\varphi)$, respectively, we can quantitatively characterize the event-by-event asymmetry in transverse energy production by considering the quantity

$$\delta E_\perp(\delta\varphi) = E_\perp^\uparrow(\delta\varphi) - E_\perp^\downarrow(\delta\varphi)\,, \tag{88}$$

and the statistical properties of transverse energy by the corresponding probability distribution

$$P(\delta E_\perp|\delta\varphi) \equiv \frac{\mathrm{d}w\big(\delta E_\perp(\delta\varphi)\big)}{\mathrm{d}\,\delta E_\perp(\delta\varphi)}\,. \tag{89}$$

This distribution was calculated [64] in the HIJING model for central Au – Au collisions at the RHIC energy $\sqrt{s} = 200\,\mathrm{GeV}$ and central Pb – Pb collisions at the LHC energy $\sqrt{s} = 5.5$ TeV for $\delta\varphi = \pi$. The distributions $P(\delta E_\perp|\pi)$ were calculated both at the partonic level and at the level of final hadrons with semihard interactions and quenching on and off.[11] This allowed analyzing the contribution of HIJING minijets and of the effects related to their hadronization to the asymmetry in question. The resulting distributions are plotted in Figs 3 and 4, for RHIC and LHC energies, respectively, with quenching turned on and the value of the minijet infrared cutoff $p_0 = 2$ GeV .

The numerical values of the mean square deviation $\delta E_\perp$ characterizing the widths of the corresponding probability distributions in Figs 3 and 4 are given in Table 1, where for completeness we also give the widths of the probability distributions with quenching turned off and for a larger value of the infrared cutoff $p_0 = 4\,\mathrm{GeV}$.

From the results presented in Figs 3 and 4 and Table 1, we can draw the following conclusions.

First, the magnitude of the azimuthal asymmetry characterized by the width of the probability distribution $P(\delta E_\perp|\delta\varphi) = \mathrm{d}w(\delta E_\perp(\delta\varphi))/\mathrm{d}\delta E_\perp(\delta\varphi)$ is strongly dependent on semihard interactions (minijets). Switching off minijets, i.e., accounting for soft mechanisms only, leads to a substantial narrowing of the asymmetry distribution, by the respective factors 2.3 at RHIC and 4.1 at the LHC energy (these values correspond to the case of quenching turned on).

Second, a remarkable fact is that parton and final (hadronic) distributions of $\delta E_\perp$ in both cases practically coincide. This means that partonic and hadronization contributions to the transverse energy flow are additive. In addition, there exists an azimuthal symmetry of the energy flow with respect to the oppositely oriented cones. Both conclusions show that the energy – energy correlation in Eqn (88) is a sensitive indicator of the presence of initial

[11] By quenching, we here understand the effect of minijet damping in the medium created after the nuclear collision.

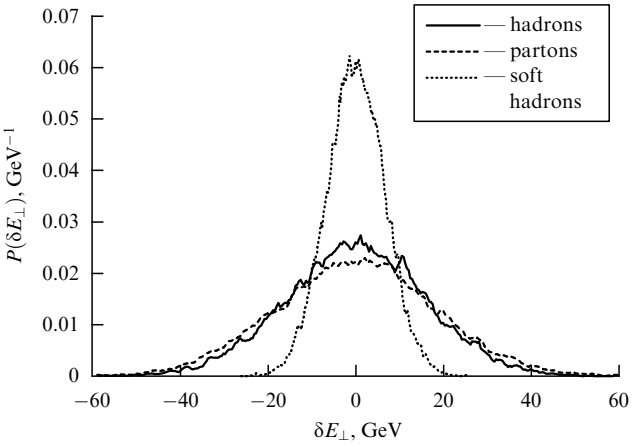

Figure 3. Probability distribution for azimuthal transverse energy disbalance in the unit rapidity window for Au – Au collisions at the RHIC energy $\sqrt{s} = 200$ GeV, $p_0 = 2$ GeV, quenching on.

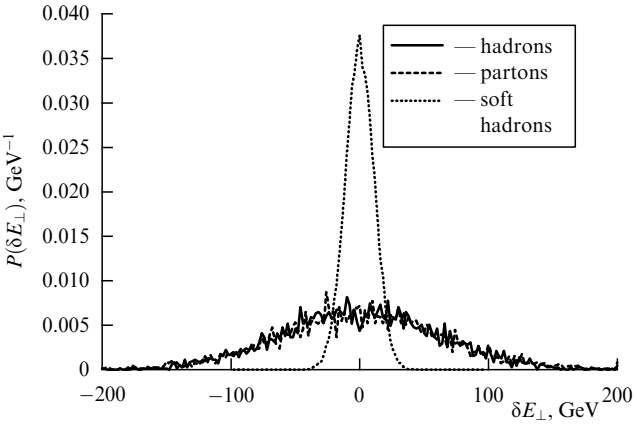

Figure 4. Probability distribution for azimuthal transverse energy disbalance in the unit rapidity window for Pb – Pb collisions at the LHC energy $\sqrt{s} = 5.5$ TeV, $p_0 = 2$ GeV, quenching on.

Table 1. The main properties of the azimuthal asymmetry of the transverse energy flux.

Nuclear collisions	$\sqrt{s}$, GeV	Infrared cutoff p_0, GeV	Asymmetry	$\sqrt{\langle\delta E^2\rangle}$, GeV
Au – Au	200	2	Hadrons (quenching on)	16
			Hadrons (quenching off)	17
			Partons	18
			Soft hadrons	7
Pb – Pb	5500	2	Hadrons (quenching on)	61
			Hadrons (quenching off)	71
			Partons	65
			Soft hadrons	15
Pb – Pb	5500	4	Hadrons (quenching on)	69
			Partons	76
			Soft hadrons	16

parton dynamics that can be studied in the calorimetric measurements in central detectors at RHIC and LHC.

Third, as expected, turning off quenching somewhat enhances the fluctuations. However, as seen from the table, the effect is insignificant numerically, giving an additional argument for the proposed asymmetry being in fact essentially determined by the earliest stage of the collision at which the primordial parton flow is formed.

Finally, we can conclude from Table 1 that the studied asymmetry is not particularly sensitive to changes in the value of the infrared cutoff p_0, thus providing a robust signal for the presence of semihard dynamics and deserving experimental study.

4.1.3 Turbulence of initial gluons: the impact parameter plane picture. In Section 4.1.2, we discussed an event-by-event asymmetry of the transverse energy flow from the 'momentum' standpoint. In a more detailed analysis, a spatial pattern giving rise to this energy–momentum flux should be considered. Of particular interest is an event-by-event transverse energy generation pattern in the impact parameter plane. This question was first addressed in Ref. [66], where strikingly interesting results were obtained .

The event-by-event transverse energy release pattern in the mixed-type models like HIJING is determined by two major factors. The first one is a distribution of the number of soft and (semi)hard inelastic collisions per unit transverse area. The second is the shape of the corresponding transverse momentum (energy) spectra. A convolution of the two distributions determines the shape of the transverse momentum and energy release. For broad distributions, one expects an intermittent turbulent spatial transverse energy distribution in the transverse plane. Most promising in this respect is of course the semihard partonic component. The distribution of the number of semihard inelastic interactions is quite broad, and the transverse energy spectra generated in these collisions are power-like. Precisely this combination leads to the intermittent turbulent-like pattern of the primordial transverse energy release [66].

In Ref. [66], the following transverse energy distribution for an ensemble of free-streaming gluons (taken from the HIJING parton event list) at zero rapidity $y = 0$ (and thus at $z = 0$) at proper time τ was considered:

$$\mathcal{E}(\tau, x_\perp, z = 0) = \sum_k \frac{p_{\perp k}}{\tau} \frac{(\tau p_{\perp k})^2}{1 + (\tau p_{\perp k})^2} \delta\big(x_\perp - x_{\perp k}(\tau)\big)\, \delta(y_k)\,, \tag{90}$$

where summation is over partons and the second factor on the right-hand side stands for the parton formation probability distribution.

It is reasonable to consider the transverse energy distribution at some coarse-grained spatial scale. More specifically, the size of the transverse cell is limited from below by the uncertainty principle $\delta r_\perp > 1/\delta p_\perp$ and from above by causality (the local horizon of the gluon in the comoving frame). At a given τ, this upper bound is simply given by $\delta r_\perp < \tau$, and therefore the number of independent cells in the transverse plane can be quite large for large nuclei and small proper times. The natural longitudinal size of the cell can be chosen as $|y| < 1$.

The particular case considered in Ref. [66] was Au–Au collisions at the RHIC energy $\sqrt{s} = 200$ GeV. The 'snapshot' of the transverse energy and transverse momentum distributions made at $\tau = 0.5$ fm gave striking results. As has been already mentioned, the HIJING model involves a well-articulated separation of the soft and semihard mechanisms of transverse energy production. We let the corresponding contributions be denoted by $\mathcal{E}_{\rm soft}$ and $\mathcal{E}_{\rm hard}$. In these terms, the results in Ref. [66] can be described as the appearance, on the background of the smooth uniformly distributed energy density $\mathcal{E}_{\rm soft} \simeq 5$ GeV, of the pronounced peaks ('hot spots') with large energy densities $\mathcal{E} > 20$ GeV (corresponding to $\mathcal{E}_{\rm hard} \geqslant 15$ GeV) separated by distances of the order of 4–5 fm. We note that the vector field of transverse momenta had a pronounced vorticity — a natural analogue with instabilities (turbulence) induced in the uniform 'soft' laminar flow by the minijet component was pointed out in Ref. [66].

The importance of the results in Ref. [66] lies, in our opinion, in the fact that their character is not related to the particular model considered (HIJING), the chosen collision energy, etc. As we have mentioned on many occasions in the preceding paragraphs, a consistent model of heavy-ion collisions is necessarily a mix of soft and hard mechanisms. Any such mix is to generate a turbulent-like intermittent picture analogous to the one discussed in Ref. [66].

4.2 Parton production and saturation in nuclear collisions

The cross sections describing hard processes (e.g., high-$p_\perp$ jet production) are proportional to the product of incoming partonic flows. At high energies, when the saturation phenomenon becomes important, this customary picture has to be reconsidered. The corresponding analysis was first made in Ref. [57], where it was shown, in particular, that because of saturation, the multiplicity and transverse energy density of gluons produced at central rapidity are characterized by the following scaling dependences on $Q_{\rm s}$:

$$\begin{aligned} \frac{{\rm d}N}{{\rm d}y} &= 2AxG_{\rm nucleon}(x, Q_{\rm s}^2)\,, \\ \frac{{\rm d}E_\perp}{{\rm d}y} &= 2Q_{\rm s}xG_{\rm nucleon}(x, Q_{\rm s}^2)\,, \end{aligned} \tag{91}$$

where $Q_{\rm s} \sim \alpha A/R^2$ is a characteristic saturation scale at which gluon emission and recombination balance each other. We see that the A-counting in Eqn (91) is different from the naively expected perturbative factor A^2, and is more akin to the one in soft production models.

It is important to stress that a picture of gluon production, and thus of the initially produced gluonic configuration, depends on the gauge used in the calculation. This fact was explicitly demonstrated in Ref. [69], where a calculation of the spectrum of gluons produced in p–A collisions was performed in both covariant and light-cone gauges. It turned out that the *origin* of the A-dependent effects looks completely different in these two gauges: in the covariant gauge, it is a rescattering of the produced gluon on the nucleons in the nucleus, and in the light-cone gauge, it is a nonlinear interaction of gluons in the nuclear wave function. This explains a certain ambivalence with which intuitive reasoning explaining the basic features of gluon production is formulated (see, e.g., Ref. [68]). Here, it is convenient to follow the 'light-cone-gauge logic', in which the number of produced gluons is roughly proportional to their 'prescattering' number in the nuclear wave function [68].

4.2.1 Spectrum of produced gluons: analytic results. The qualitative ideas described in Section 4.2 were further

developed in Ref. [70], where an analytic nonlinear ansatz for the spectrum of gluons produced in the collision of two identical nuclei was suggested. The corresponding expression can be written as a two-dimensional integral in the transverse coordinate plane [70]. With logarithmic accuracy and for parametrically small transverse momenta $k_\perp^2 < Q_s^2$, one can perform the two-dimensional integration over the coordinates and obtain the following impressively simple expression for the gluon spectrum:

$$\frac{dN^{A-A}}{d^2b\,dy\,d^2k_\perp} = \frac{C_F}{\alpha\pi^3}\frac{Q_s^2}{k_\perp^2}\left[\exp\left(-\frac{k_\perp^2}{2Q_s^2}\right) - \exp\left(-\frac{k_\perp^2}{Q_s^2}\right)\right]. \quad (92)$$

Equation (92) implies the important conclusion that up to possible logarithmic factors neglected in the process of its derivation, the spectrum of gluons produced in nucleus–nucleus collision is *finite* in the limit as $k_\perp^2/Q_s^2 \to 0$,

$$\frac{dN^{A-A}}{d^2b\,dy\,d^2k_\perp} \to \frac{1}{\alpha}\frac{C_F}{2\pi^3}, \quad (93)$$

providing, therefore, infrared-finite results for expressions containing integration over transverse momenta such as the inelastic cross section. This result is highly nontrivial. In the standard minijet scenarios based on collinear factorization, infrared finiteness can be ensured only by using brute force (an explicit infrared cutoff for a strongly divergent spectrum $\sim 1/k_\perp^4$). In p–A scattering, where nonlinear corrections related to the single participant nucleus are summed, the gluon spectrum still has a power-like divergence at small momenta ($\sim 1/k_\perp^2$) [25, 70]. This shows that it is only the combination of all nonlinear effects in both colliding nuclei that ensures the infrared finiteness of the spectrum of produced gluons and of the physical cross sections calculated from it.

The spectrum of Eqn (92) allows making quantitative estimates relating the physical quantities to the saturation momentum more precise. In particular, the mean transverse momentum of produced gluons is given by

$$\langle k_\perp^2\rangle = \frac{1}{\ln 2}\,Q_s^2. \quad (94)$$

We see that the numerical value of $\langle k_\perp^2\rangle$ is indeed very close to that of Q_s^2, as was assumed in the intuitive picture considered in Refs [23, 57, 68]. Performing integration over $k_\perp$ in Eqn (92), we obtain an expression for the gluon rapidity density in the transverse plane,

$$\frac{dN^{A-A}}{d^2b\,dy} = \frac{1}{\alpha}\frac{\ln 2\,C_F}{\pi^2}\,Q_s^2. \quad (95)$$

It is useful to compare Eqn (95) with the expression for the density of gluons in the nuclear wave function calculated in the same cylindrical geometry in the McLerran–Venugopalan approximation:

$$\frac{dN^{MW}}{d^2b\,dy} = \frac{1}{\alpha}\frac{C_F}{2\pi^2}\,Q_s^2. \quad (96)$$

Comparing Eqn (95) with Eqn (96), we see that the density of *produced* gluons, Eqn (95), is indeed proportional to the density of gluons in the nuclear wave function

$$\frac{dN^{A-A}}{d^2b\,dy} = 2\ln 2\,\frac{dN^{MW}}{d^2b\,dy}, \quad (97)$$

with the proportionality coefficient $2\ln 2 \simeq 1.39$. From Eqn (95), we can also obtain the rapidity density of the produced gluons in terms of the nucleon structure function,

$$\frac{dN^{A-A}}{dy} = \pi R_A^2\,\frac{1}{\alpha}\frac{\ln 2\,C_F}{\pi^2}\,Q_s^2 = 2\ln 2(V_A\rho)xG(x,Q_s^2), \quad (98)$$

where $V_A \sim A$ is a nuclear volume.

4.2.2 Parton production and saturation: numerical solution. A natural problem arising within the context of the McLerran–Venugopalan approach to high-energy heavy-ion physics is to study, at the same semiclassical level, the spectrum of gluons produced in collisions of two nuclei. Evidently, the spectrum of created gluons depends on the gluon mode content in colliding nuclei [67]. In the pioneering paper [67], the spectrum of produced gluons was calculated to the leading order in the perturbation theory. The answer contained a characteristic strong infrared divergence. Later, these calculations were expanded in Refs [71–73]. In this approach, the problem is to solve the Yang–Mills equations in the presence of the external source current [67]

$$J^\mu = \delta^{\mu+}\rho_{(1)}\delta(x^-) + \delta^{\mu-}\rho_{(2)}\delta(x^+) \quad (99)$$

corresponding to the two incident nuclei. In Refs [74–81], an extensive program for the numerical solution of this problem was realized. Under the assumption of the invariance under longitudinal Lorentz boosts, the problem reduces to solving the $(2+1)$ classical Hamiltonian chromodynamics on the lattice.

The result depends on three parameters — the charge g, the color charge density μ_A [cf. (24)], and the nuclear radius R_A — through their dimensionless combination $\xi = g^4\pi R_A^2\mu_A^2$. Correspondingly, for the rapidity density of multiplicity and the transverse energy of primordial glue, we have

$$\frac{dE_\perp}{dy} = \mu_A\xi f_E(\xi), \qquad \frac{dN}{dy} = \xi f_N(\xi). \quad (100)$$

In the weak-field limit (more exactly, for $\xi < 50$), all considered quantities are characterized by a strong dependence on ξ and thus on the infrared cutoff. At $\xi \sim 100$, this dependence is saturated.

It is important to check whether the perturbative result in Ref. [67] is reproduced in the weak-field limit. A recent analysis shows that the agreement can be reached only at very small values of the scaling parameter $\xi < 10$ [81]. As regards the spectrum of produced gluons, it has an exponential 'thermodynamical' form at small energies [77, 81], but deviates from it at large energies [81].

The most important issue addressed by the numerical computation is, probably, how large the occupation numbers of gluon modes f_g are. The classical description on which the considered method is based is valid only at large $f_g \gg 1$. The situation here is not yet finally settled, but it is most probable that for parameter values corresponding to RHIC energies, a statement on the fulfillment of the condition $f_g \gg 1$ would be an exaggeration.

4.2.3 Interpreting RHIC data in color glass condensate terms. With publications of experimental data obtained at RHIC, there arises a possibility of testing the ideas related to CGC

(saturation) physics in the framework of simplest model assumptions. We assume that from the moment the CGC melts, because of collision, into the physical gluon modes, the produced gluons no longer interact and their transformation into final hadrons is not accompanied by substantial changes in the kinematic structure of the energy–momentum flow (soft hadronization hypothesis). Then, by making comparisons with experimental data on charged multiplicity [82–85] or multiplicity per participant [82], we can establish constraints on parameters describing the initial configuration of produced gluons.

For example, we consider a model with the cylindrical nuclear geometry used in Ref. [70]. Then, e.g., taking the value for the charged multiplicity density measured by PHOBOS in Au–Au collisions [100]

$$\left.\frac{\mathrm{d}N_{\mathrm{ch}}^{\mathrm{Au-Au}}}{\mathrm{d}\eta}\right|_{\eta=0} = 555 \pm 12(\mathrm{stat}) \pm 35(\mathrm{syst})\,, \tag{101}$$

and taking $\alpha_{\mathrm{s}} = 0.3$ and $\pi R_A^2 = 150$ fm^2, we obtain the estimate for the saturation momentum Q_{s} from Eqn (98) as $Q_{\mathrm{s}}^2 \approx 0.7$ GeV^2.

Analogously, we can compare the experimental data of the results of the numerical analysis described in Section 4.2.2. For example, using the second equation in (100), we can determine (for given g and R_A) the value of μ and compute the transverse energy density from the first equation in (100). Using [81] $\mathrm{d}N/\mathrm{d}y \approx 1000$, we obtain (for $g = 2$ and $S_A = 150$ fm^2) $\mu = 0.5$ GeV and $\mathrm{d}E_\perp/\mathrm{d}y = 1.5$ [GeV] $\times\, \mathrm{d}N/\mathrm{d}y$.

A more elaborate way of estimating the characteristics of CGC from experimental data was suggested in Refs [86–88]. The main novelty of this approach is to use the density of participating nucleons in the formula determining the saturation scale,

$$Q_{\mathrm{s}}^2(s_\perp, b_\perp) = \frac{4\pi^2 N_{\mathrm{c}}}{N_{\mathrm{c}}^2 - 1}\,\alpha_{\mathrm{s}}(Q_{\mathrm{s}}^2)\,xG(x, Q_{\mathrm{s}}^2)_{\mathrm{nucleon}}\,\frac{\rho_{\mathrm{part}}(s_\perp, b_\perp)}{2}\,, \tag{102}$$

where $\rho_{\mathrm{part}}(s_\perp, b_\perp)$ is the density of participant nucleons as a function of the collision impact parameter $b_\perp$ and the coordinate in the transverse plane $s_\perp$. The substitution of ρ_{part} into the equation determining the saturation scale presents a highly nontrivial hypothesis on the nonperturbative geometry of the gluon production mechanism. The resulting relation between multiplicity per participant and saturation momentum is given by [86–90]

$$\left\langle \frac{2}{N_{\mathrm{part}}}\,\frac{\mathrm{d}N_{\mathrm{ch}}}{\mathrm{d}y} \right\rangle \simeq \frac{2}{3}\,c\,xG\big(x, \langle Q_{\mathrm{s}}^2\rangle\big)\,, \tag{103}$$

where c is the proportionality coefficient between the gluon spectrum and the nuclear wave function discussed in Section 4.2.1 and $\langle Q_{\mathrm{s}}^2\rangle$ denotes averaging over the impact parameter. Experimentally, $(2/N_{\mathrm{part}})\,\mathrm{d}N_{\mathrm{ch}}/\mathrm{d}y \simeq 3.8$, and therefore Eqn (103) allows estimating the (average) saturation momentum Q_{s}. Without invoking additional assumptions, the typical value of Q_{s}^2 obtained from Eqn (103) is not too big: $Q_{\mathrm{s}}^2 \simeq 0.5{-}0.7$ GeV^2.

4.3 Interaction effects. On the way to thermalization?

Up to now, we have discussed only the properties of the initially produced gluon system appearing immediately after the coherence of the wave functions of incident nuclei is broken by the collision and, as a consequence, entropy in the form of physical (mainly gluonic) fields is produced. Before the energy–momentum flow of these fields is converted into that of final hadrons hitting detectors, it could, however, be essentially transformed by interaction effects. The question that has particularly shaped high-energy heavy-ion physics is whether the reinteraction of produced parton matter could lead to its thermalization and the formation of quark–gluon plasma, thus allowing us to reproduce, in the laboratory, conditions that existed in the early universe. In this subsection, we briefly review the recent progress in describing the real-time evolution of an interacting (dense) gluon system.

Broadly speaking, the reinteraction effects can be classified into two categories.

First, if a strong *physical* gluon field is produced, it can evolve (in real time) according to the nonlinear Yang–Mills equations of motion. This regime is possible until the occupation numbers of the field modes become small. Schematically, the occupation numbers f should satisfy the inequality $1 < f < 1/\alpha_{\mathrm{s}}$. Such nonlinear evolution could, in principle, lead to all kinds of exciting scenarios typical for nonlinear field dynamics — from the appearance of collective dynamical instabilities to chaotization and the formation of localized collective excitations.

Second, the reinteraction of produced physical gluons can be described in terms borrowed from kinetic theory.[12] This possibility has been discussed, in relation to saturation physics in nuclear collisions, in a number of recent publications [89, 91–93, 103].

The simplest way to analyze gluon reinteraction effects is to use the Boltzmann equation formalism at a binary scattering level [91–93]. Calculations of the equilibration time in this approximation produce a parametrically large estimate $\tau_{\mathrm{eq}} \sim \exp\left(1/\sqrt{\alpha_{\mathrm{s}}}\right) 1/Q_{\mathrm{s}}$. The equilibration rate is low because the momentum transfer in the system is not effective: the transverse momenta exchanged in the gluon interactions are small — of the order of the infrared cutoff (the screening Debye mass).

The main motivation for developing the saturation physics approach is the very dense system of primordial gluons that is, presumably, formed at the initial stage of high-energy heavy-ion collision. To produce a more reliable description for gluon reinteraction and their possible equilibration, a kinetic approach that is more appropriate for (initially) dense systems is required. Such an approach was developed in Refs [89, 103], where the kinetic equation formalism taking inelastic processes into account in the third order in gluon density was constructed and employed. The resulting reinteraction scenario described in Refs [89, 103] is quite complex and involves several stages, to which there correspond a set of proper time scales $\tau \sim (\tau_0, \alpha_{\mathrm{s}}^{-3/2}\tau_0, \alpha_{\mathrm{s}}^{-5/2}\tau_0, \alpha_{\mathrm{s}}^{-13/5}\tau_0)$, where $\tau_0 = 1/Q_{\mathrm{s}}$.

Initially, at $\tau \sim \tau_0$, physical gluons are freed from the nuclear wave functions and form a dense system of semihard gluons with transverse momenta of the order of Q_{s} and the occupation number of the order of $1/\alpha_{\mathrm{s}}$. The system expands, and at $\tau \sim \alpha_{\mathrm{s}}^{-3/2}\tau_0$, the occupation numbers of semihard primordial gluons become small, and hence the standard description in terms of the Boltzmann equation can be applied.

[12] There are good grounds to believe that these two approaches are (at least partially) complementary [102].

In the interval of proper times $\alpha_s^{-3/2}\tau_0 < \tau < \alpha_s^{-5/2}\tau_0$, inelastic interactions of semihard gluons lead to the appearance of soft gluons with momenta $k_\perp \sim \alpha_s^{1/2}$. At the end of this interval, the densities of hard and soft gluon components equalize.

At $\tau > \alpha_s^{-5/2}\tau_0$, a thermalization of the soft gluon subsystem occurs. Its temperature subsequently undergoes a linear increase through the energy loss of the remaining semihard modes in the hot soft gluon medium until at $\tau \sim \alpha_s^{-13/5}\tau_0$, it reaches its maximal value $T \sim \alpha_s^{2/5} Q_s$. At this timescale, semihard gluons disappear and the gluon system is fully equilibrated.

Detailed discussion of RHIC data in the context of the above-described scenario can be found in Ref. [89].

We note that the validity of the scenario described in [89, 103] is based on some quite restrictive assumptions. For example, for the equilibration time $\alpha_s^{-13/5}\tau_0$ to be less than the 'binary' one, $\exp(1/\sqrt{\alpha_s})$, the coupling constant should be very small, $\alpha_s < 0.004$. Also — especially at RHIC energies, when $Q_s \sim 1\ \text{GeV}^2$ and realistic values of the coupling constant $\alpha_s \sim 0.3$ — the transverse momenta of the soft gluons produced at the second stage $k_\perp \sim \alpha_s^{1/2}\tau_0$ are in fact of the order of Λ_{QCD}, and therefore perturbative methods could turn out to be insufficient.

5. Conclusion

In this review, we have discussed some aspects of the exciting and rapidly developing domain of the application of nonlinear QCD physics to a description of ultrarelativistic heavy-ion collisions. Research in this field is related to fundamental theoretical questions such as unitarity of strong interactions at high energies, at the same time providing the possibility of explaining the experimental data, currently for the RHIC accelerator, as well as for the expected extremely interesting experimental data from the LHC.

Acknowledgements

I am grateful to I M Dremin, E Iancu, A Kovner, Yu Kovchegov, L McLerran, and I I Royzen for reading the manuscript and useful comments and suggestions. The work was supported by the RFBR grants 04-02-16880 and 02-02-16779 and the Scientific Schools Support Grant 1936.2003.02.

References

1. Iancu E, Leonidov A, McLerran L, in *QCD Perspectives on Hot and Dense Matter* (NATO Sci. Series, Ser. II, Vol. 87, Eds J-P Blaizot, E Iancu) (Dordrecht: Kluwer Acad. Publ., 2002) p. 73; hep-ph/0202270
2. Iancu E, Venugopalan R, in *Quark Gluon Plasma 3* (Eds R C Hwa, X-N Yang) (Singapore: World Scientific, 2002) p. 249; hep-ph/0303204
3. McLerran L, hep-ph/0402137
4. Wang X-N *Phys. Rep.* **280** 287 (1997)
5. Kaĭdalov A B, Ter-Martirosyan K A *Yad. Fiz.* **40** 211 (1984) [*Sov. J. Nucl. Phys.* **40** 135 (1984)]
6. Kaidalov A B *Surv. High Energy Phys.* **13** 265 (1999); *Nucl. Phys. B: Proc. Suppl.* **75** 81 (1999)
7. Royzen I I, Feĭnberg E L, Chernavskaya O S *Usp. Fiz. Nauk* **174** 473 (2004) [*Phys. Usp.* **47** 427 (2004)]
8. Emel'yanov V M, Timoshenko S L, Strikhanov M N *Vvedenie v Relyativistskuyu Yadernuyu Fiziku* (Introduction to Relativistic Nuclear Physics) (Moscow: Fizmatlit, 2004)
9. Khoze V A, Ochs W *Int. J. Mod. Phys. A* **12** 2949 (1997)
10. Dremin I M, Gary J W *Phys. Rep.* **349** 301 (2001)
11. Dremin I M *Usp. Fiz. Nauk* **172** 551 (2002) [*Phys. Usp.* **45** 507 (2002)]
12. Kaĭdalov A B *Phys. Usp.* **173** 1153 (2003) [*Phys. Usp.* **46** 1121 (2003)]
13. DeWolf E A, Dremin I M, Kittel W *Phys. Rep.* **270** 1 (1996)
14. Gribov V N, Lipatov L N *Yad. Fiz.* **15** 1218 (1972) [*Sov. J. Nucl. Phys.* **15** 675 (1972)]; Altarelli G, Parisi G *Nucl. Phys. B* **126** 298 (1977); Dokshitser Yu L *Zh. Eksp. Teor. Fiz.* **73** 1216 (1977) [*Sov. Phys. JETP* **46** 641 (1977)]
15. Lipatov L N *Yad. Fiz.* **23** 642 (1976) [*Sov. J. Nucl. Phys.* **23** 338 (1976)]; Kuraev E A, Lipatov L N, Fadin V S *Zh. Eksp. Teor. Fiz.* **72** 377 (1977) [*Sov. Phys. JETP* **45** 199 (1977)]; Balitskiĭ Ya Ya, Lipatov L N *Yad. Fiz.* **28** 1597 (1978) [*Sov. J. Nucl. Phys.* **28** 822 (1978)]
16. Gribov L V, Levin E M, Ryskin M G *Phys. Rep.* **100** 1 (1983)
17. Mueller A H, Qiu J-W *Nucl. Phys. B* **268** 427 (1986)
18. Frankfurt L, Strikman M *Phys. Rep.* **160** 235 (1988)
19. Levin E M, Ryskin M G *Phys. Rep.* **189** 268 (1990)
20. Lipatov L N *Phys. Rep.* **286** 131 (1997)
21. Lipatov L N *Nucl. Phys. B* **452** 369 (1995)
22. Bartels J, Lipatov L N, Vacca G P *Nucl. Phys. B* **706** 391 (2005); hep-ph/0404110
23. McLerran L, Venugopalan R *Phys. Rev. D* **49** 3352; **50** 2225 (1994)
24. Jalilian-Marian J et al. *Phys. Rev. D* **55** 5414 (1997)
25. Kovchegov Yu V, Mueller A H *Nucl. Phys. B* **529** 451 (1998)
26. Ayala A et al. *Phys. Rev. D* **52** 2935 (1995); **53** 458 (1996)
27. Jalilian-Marian J, Kovner A, Weigert H *Phys. Rev. D* **59** 014015 (1999)
28. Iancu E, Leonidov A, McLerran L *Nucl. Phys. A* **692** 583 (2001)
29. Iancu E, Leonidov A, McLerran L *Phys. Lett. B* **510** 133 (2001)
30. Ferreiro E et al. *Nucl. Phys. A* **703** 489 (2002)
31. Kovner A, Milhano J G *Phys. Rev. D* **61** 014012 (2000)
32. Jalilian-Marian J et al. *Nucl. Phys. B* **504** 415 (1997)
33. Leonidov A, in *Quantization, Gauge Theory, and Strings: Proc. of the Intern. Conf. Dedicated to the Memory of Professor Efim Fradkin, Moscow, Russia, June 5–10, 2000* Vol. 2 (Eds A Semikhatov, M Vasiliev, V Zaikin) (Moscow: Scientific World, 2001) p. 542
34. Jalilian-Marian J, Jeon S, Venugopalan R *Phys. Rev. D* **63** 036004 (2001)
35. Jalilian-Marian J et al. *Phys. Rev. D* **59** 014014 (1999)
36. Kovner A, Wiedemann U A *Phys. Rev. D* **64** 114002 (2001)
37. Mueller A H *Phys. Lett. B* **523** 243 (2001)
38. Bartels J *Nucl. Phys. B* **175** 365 (1980); Kwieciǹski J, Praszalowicz M *Phys. Lett. B* **94** 413 (1980)
39. Kovner A, Milhano J G, Weigert H *Phys. Rev. D* **62** 114005 (2000)
40. Balitsky I *Nucl. Phys. B* **463** 99 (1996)
41. Kovchegov Yu V *Phys. Rev. D* **60** 034008 (1999); **61** 074018 (2000)
42. Mueller A H *Nucl. Phys. B* **558** 285 (1999)
43. Iancu E, McLerran L *Phys. Lett. B* **510** 145 (2001)
44. Iancu E, Itakura K, McLerran L *Nucl. Phys. A* **708** 327 (2002)
45. Iancu E, Itakura K, McLerran L *Nucl. Phys. A* **724** 181 (2003); hep-ph/0212123
46. Levin E, Tuchin K *Nucl. Phys. B* **573** 833 (2000); *Nucl. Phys. A* **693** 787 (2001)
47. Rummukainen K, Weigert H *Nucl. Phys. A* **739** 183 (2004); hep-ph/0309306
48. Mueller A H, Shoshi A I *Nucl. Phys. B* **692** 175 (2004); hep-ph/0402193
49. Jalilian-Marian J et al. *Phys. Rev. D* **59** 034007 (1999)
50. Ferreiro E et al. *Nucl. Phys. A* **710** 373 (2002)
51. Kovner A, Wiedemann U A *Phys. Rev. D* **66** 051502(R) (2002)
52. Kovner A, Wiedemann U A *Phys. Rev. D* **66** 034031 (2002)
53. Kovner A, Wiedemann U A *Phys. Lett. B* **551** 311 (2003)
54. Jacob M, Landshoff P V *Mod. Phys. Lett. A* **1** 657 (1986)
55. Kajantie K, Landshoff P V, Lindfors J *Phys. Rev. Lett.* **59** 2527 (1987)
56. Eskola K J, Kajantie K, Lindfors J *Nucl. Phys. B* **323** 37 (1989)
57. Blaizot J P, Mueller A H *Nucl. Phys. B* **289** 847 (1987)
58. Wang X-N *Phys. Rev. D* **46** R1900 (1992); **47** 2754 (1993)
59. Soper D E, hep-ph/9706320
60. Leonidov A, Ostrovsky D *Eur. Phys. J. C* **11** 495 (1999)
61. Leonidov A, hep-ph/0005010
62. Wang X-N, Gyulassy M *Phys. Rev. D* **44** 3501 (1991); **45** 844 (1992); Gyulassy M, Wang X-N *Comp. Phys. Commun.* **83** 307 (1994)
63. Leonidov A V, Ostrovsky D M *Eur. Phys. J. C* **16** 683 (2000)
64. Leonidov A, Ostrovsky D *Phys. Rev. C* **63** 037901 (2001)

65. Sjöstrand T *Comp. Phys. Commun.* **82** 74 (1994)
66. Gyulassy M, Rischke D H, Zhang B *Nucl. Phys. A* **613** 397 (1997)
67. Kovner A, McLerran L, Weigert H *Phys. Rev. D* **52** 3809, 6231 (1995)
68. Mueller A H *Nucl. Phys. B* **572** 227 (2000)
69. Kovchegov Yu V, Mueller A H *Nucl. Phys. B* **529** 451 (1998)
70. Kovchegov Yu V *Nucl. Phys. A* **692** 557 (2001); **698** 619 (2002)
71. Kovchegov Yu V, Rischke D H *Phys. Rev. C* **56** 1084 (1997)
72. Matinyan S G, Müller B, Rischke D H *Phys. Rev. C* **56** 2191 (1997); **57** 1927 (1998)
73. Gyulassy M, McLerran L *Phys. Rev. C* **56** 2219 (1997)
74. Krasnitz A, Venugopalan R *Nucl. Phys. B* **557** 237 (1999)
75. Krasnitz A, Venugopalan R *Phys. Rev. Lett.* **84** 4309 (2000)
76. Krasnitz A, Venugopalan R *Phys. Rev. Lett.* **86** 1717 (2001)
77. Krasnitz A, Nara Y, Venugopalan R *Phys. Rev. Lett.* **87** 192302 (2001)
78. Krasnitz A, Venugopalan R *Nucl. Phys. A* **698** 209c (2002)
79. Krasnitz A, Nara Y, Venugopalan R *Phys. Lett. B* **554** 21 (2003)
80. Krasnitz A, Nara Y, Venugopalan R *Nucl. Phys. A* **717** 268 (2003)
81. Lappi T *Phys. Rev. C* **67** 054903 (2003)
82. Back B B et al. (PHOBOS Collab.) *Phys. Rev. Lett.* **85** 3100 (2000); **88** 022302 (2002)
83. Adcox K et al. (PHENIX Collab.) *Phys. Rev. Lett.* **86** 3500; **87** 052301 (2001)
84. Bearden I G et al. (BRAHMS Collab.) *Phys. Lett. B* **523** 227 (2001)
85. Adler C et al. (STAR Collab.) *Phys. Rev. Lett.* **87** 112303 (2001)
86. Kharzeev D, Nardi M *Phys. Lett. B* **507** 121 (2001)
87. Kharzeev D, Levin E *Phys. Lett. B* **523** 79 (2001)
88. Kharzeev D, Levin E, Nardi M, hep-ph/0111315
89. Baier R et al. *Phys. Lett. B* **539** 46 (2002)
90. Mueller A H *Nucl. Phys. A* **715** 20 (2003); hep-ph/0208278
91. Mueller A H *Phys. Lett. B* **475** 220 (2000)
92. Bjoraker J, Venugopalan R *Phys. Rev. C* **63** 024609 (2001)
93. Serreau J, Schiff D *J. High Energy Phys.* **11** 039 (2001)
94. Weigert H *Nucl. Phys. A* **703** 823 (2002)
95. Mueller A H *Phys. Lett. B* **523** 243 (2001)
96. Braun M *Eur. Phys. J. C* **16** 337 (2000)
97. Golec-Biernat K, Wüsthoff M *Phys. Rev. D* **60** 114023 (1999)
98. Wang X-N, Gyulassy M *Phys. Rev. Lett.* **86** 3496 (2001)
99. Banner M et al. (UA2 Collab.) *Phys. Lett. B* **118** 203 (1982)
100. Kunszt Z, Soper D E *Phys. Rev. D* **46** 192 (1992)
101. Sjöstrand T, van Zijl M *Phys. Rev. D* **36** 2019 (1987)
102. Mueller A H, Son D T *Phys. Lett. B* **582** 279 (2004); hep-ph/0212198
103. Baier R et al. *Phys. Lett. B* **502** 51 (2001)